The definitive publisher version is available online at https://doi.org/10.1016/j.jclepro.2022.131842

Cleaner and safer disposal of electrolytic manganese resides in cement-based materials using direct electric curing

Fan Wang[a], Guangcheng Long[a], Min Bai[a], Jilin Wang[a], Zhihan Yang[a], Xiang Zhou[a], John L. Zhou[a,b]

[a]School of Civil Engineering, Central South University, 68 South Shaoshan Road, Changsha, Hunan, 410075, China

[b]Centre for Green Technology, School of Civil and Environmental Engineering, University of Technology Sydney, Sydney, NSW, 2007, Australia

Highlights

- cement hardening with DEC realizes high dose hazard-free disposal of EMR.
- DEC promotes cement hydration with high-early strength and EMR solidification with respect to IC.
- The improvement in strength of paste cured in DEC is boosted by ionic migration and pore structure.
- High DEC voltage promotes the cement hydration and ettringite and portlandite formation.
- Mn^{2+} and NH_4^+-N below national standards at high-alkali condition from cement hydration.

Graphical abstract

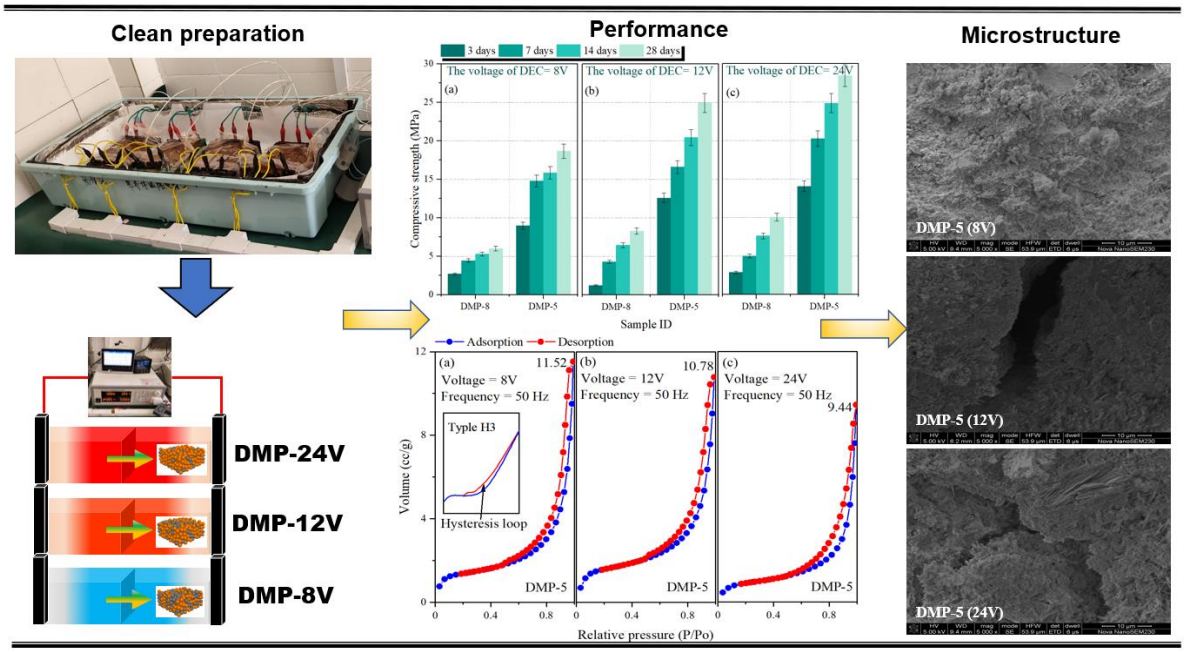

Abstract

The direct stockpiling of electrolytic manganese resides (EMR) poses a major environmental issue, and more eco-friendly disposal is urgently needed.. The combination of cement hardening and direct electric curing (DEC) provides a potential solution for hazard-free disposing EMR. The effects of DEC voltages and cement amount on mechanical properties, hydrated products, pore structure of cement-EMR paste were investigated. The influencing mechanism of DEC on the properties of cement was explored in-depth using TG and XRD results. The environmental and economic evolution of DEC was analyzed, and the leaching test was conducted to evaluate the immobilization of heavy metal. Results indicate that cement-EMR pastes cured in higher DEC and increasing cement equivalent can increase mechanical strength and improve pore structure and capillary water absorption with respect to that cured in IC. The increase in cement equivalent can improve cement hardening effect, and the increased voltage enhances the ionic driving force. The boosted ettringite formation occurs in cement-EMR paste after introducing DEC and amplifying the DEC voltage. The improvement of ion concentration in DEC accelerats the hydration products. The EIF and CIF values of pastes DMP-5 cured in 12V-DEC exhibit the lowest values with respect to curing in other voltage and IC. The decrease in the leaching amount of Mn^{2+} and NH_4^+-N as the DEC voltage increase, and the 28-d results showed that Mn^{2+} and NH_4^+-N in pastes were in accordance with the leaching national standards (GB 8978-1996). The incorporation of DEC and cement-solidified disposal for EMR could provide a potential solution for high-value and large-capacity disposal of hazardous solid waste.

Keywords: Direct electric curing; Cement hardening; Electronic manganese resides; Hazard-free disposal; High-added utilization; Environmental and economic evaluation

1. Introduction

Electrolytic manganese resides (EMR) are a kind of hazardous solid waste produced by a traditional hydrometallurgy process with rhodochrosite ore as the primary raw material through sulfuric acid leaching-electrowinning (Duan et al., 2010; Wang et al., 2020). Currently, wet-smelting one ton of electrolytic manganese produces 10-14 tons of EMR (Shu et al., 2016; Wang et al., 2019; Shu et al., 2019). This condition has been rapidly exacerbated by the continued depletion of global raw ore because of over-exploitation (Duan et al., 2011; He et al., 2021a). As the decades of development, China now has more than 160 million tons of EMR stockpiles, whereas producing more than 10 million tons of new-forming EMR annually (Xu et al., 2014; Zhou et al., 2014; Li et al., 2020; Han and Wu, 2019; He et al., 2021b). However, most electrolytic manganese smelters stacked dispose their EMR directly in designated waste landfill sites without high-quality pretreatment (Duan et al, 2011; Wang et al., 2020; Zhang et al., 2020a). Meanwhile, as the untreated stockpiled EMR generally exposed to the open air for long time, inevitably that not only causes serious pollution in the groundwater, soil, air and ecosystems, but also poses a rock-ribbed threat to the health and survival environment (Han and Wu, 2019). The stacked EMR significantly hindered the exploitation of the manganese smelters and posed a serious threat to the manganese ore development (Wang et al., 2016; Li et al., 2018; Sun et al., 2020). Therefore, EMR has attracted widespread concern in society, and need to be solved urgently. Therefore, the realization of hazard-free disposal and resource utilization of EMR is the key to the sustainable development of electrolytic manganese metal industry.

In China, the production of electrolytic manganese metal uses rhodochrosite as raw materials (Zhang and Cheng, 2007; Han et al., 2018; He et al., 2021c). The whole production of electrolytic manganese metal is mainly divided into the following procedures (Duan et al., 2011; Xu et al., 2014). a) The crushed rhodochrosite and sulfuric acid solution are mixed based on a liquid/solid ratio of 8-10 L/kg. The initial concentration of sulfuric acid solution is set as 70-80 g/L, and then the samples are leached in 80-85 ℃ for 3-6 h. b) The pyrolusite is used to oxidize the dissolved ferrous ions, followed by the addition of ammonium hydroxide for adjusting the pH of the slurry to 6.5-7.0. In this slurry, the iron ions are deposited together with other heavy metal ions and acid soluble silicon. c) Then, pressure filtration is used to separate solid residues from solution. A vulcanizer is employed to removal heavy metals, and the purification solution and vulcanized reside are formed by pressure filtration. Finally,

EMR is obtained which refers to the filter residue obtained in sulfuric acid leaching, iron removal and sedimentation procedures in the electrolytic manganese metal production process (Wang et al., 2013). Therefore, EMR is classified as general industrial solid waste, but contains a large amount of soluble salts, i.e., ammonium sulfate and manganese sulfate, and many heavy metals including Zn, Cu and Mn, etc (He et al., 2021c; Shu et al., 2020; Ma et al., 2020; Wang et al., 2020). Moreover, it is noted that the EMR is a mixture of hazardous solid waste and obtained from different procedures instead of only from the exhibited leaching procedure (Zhang et al., 2019a and 2019b; Zhang et al., 2020b).

Cement hardening as a stabilization/solidification technology was successfully employed for solid waste disposal (Chen et al., 2020; Han et al., 2020; He et al., 2021d; Lan et al., 2021). The cement hardening is also widely utilized in soil remediation around the world (Tang et al., 2020). The main reason is that cement hardening provides high-efficiency of remediation and high-effective prevention of the release in harmful chemicals in hazardous wastes (Wang et al., 2013; Wang et al., 2018). Such an approach has been employed rapidly in China in recent years (Xu et al., 2019). Cement hardening is associated with the development of physicochemical processes (i.e., cement hydration, cation exchange, flocculation and agglomeration, and carbonation) (Senneca et al., 2020). Alkaline environment and cement hydration provided by cement hardening could convert soluble harmful substances into insoluble or thermodynamically stable substances, including hydroxide, carbonate, sulfate and silicate precipitates (Zhan et al., 2019). The transformation can decrease the migration and diffusion of toxic components. Jiang et al. (2018) solidified EMR with cement and other solid waste, and the toxicity leaching concentration in solution via cement hardening significantly decrease to 0.022 mg/L. Li et al (2016). also used cement for disposing EMR, and achieved a manganese curing rate of 99% and a leaching concentration of manganese of 0.515 mg/L. In addition, the cement hydration reaction can solidify EMR into hydration products during the hydration process. However, these disposals use a significant amount of cement equivalent, resulting in lower EMR consumption efficiencies and high disposal costs. Safe and low-cost improvement of EMR consumption efficiency is an urgent problem to deal with the current massive EMR stockpiling.

Microwave curing and direct electric curing (DEC), as the main representatives of volume heating methods, can directly alter the movement modes of free ions in fresh slurry and promotes the cement hydration significantly by temperature rising and ionic driving force (Makul et al., 2017; Koh et al.,

2019). DEC emphatically uses Joule heating generated by electric current from fresh specimens with low resistivity to accelerate cement hydration and improve early mechanical properties (Yang et al., 2021). The energy efficiency of volume heating methods is much greater than that of surface heating methods (Yang et al., 2021; Ma et al., 2021). Meanwhile, the external and internal temperature of slurry is no significant difference, and then the mechanical properties, durability and microstructure of slurry have not sustained the negative effects (Shi et al., 2019). Therefore, volume heating methods are the promising and potential curing regimes for preparing cement-based material with high early-strength. Specifically, DEC was firstly employed in fabricating the railway sleeper, and later in production of fiber-reinforced concrete, geopolymers and intelligent concrete (Kovtun et al., 2016; Cecini et al., 2018). DEC for a certain time significantly enhances the early-age strength, and the improvement in 28-d strength is also considerable. Previous studies on the application of DEC in-situ construction have found that DEC has a high convenience in-situ (Wadhwa et al., 1987). Although DEC is a successful technique for the preparation of cement-based material with high early-strength, more researches are needed to investigate the influences of DEC on hydration process and products, microstructure of cement solidified waste materials.

In this study, cement hardening in combination with direct electric curing (DEC) provides a potential solution for clean disposal of EMR. Effects of DEC voltages and cement equivalents on mechanical properties, hydrated products, pore structure of cement-EMR paste were investigated. The influencing mechanism of DEC on the properties of cement was explored in-depth using TG and XRD results. The environmental and economic evolution of DEC was analyzed, and the leaching test was conducted to evaluate the immobilization of heavy metal. Finally, the thermal effect and the mechanism of cement-EMR pastes cured in DEC were discussed. The incorporation of DEC in cement-solidified disposal for EMR could provide a solution for clean and large-capacity disposal of hazardous solid waste.

2. Methodology

2.1 Materials

The cement pastes were prepared for each measurement. The d cement (produced by Southern Cement Co., Ltd) is classified as P.I. 42.5R ordinary Portland cement (OPC) according to Chinese standard, and the main properties and oxide compositions are presented in Table 1 and Table 2. Besides,

the used EMR (obtained by Xiangtan Electrochemical Group) is formed from two ore one-step process, and the oxide compositions is also exhibited in Table 2. Prior to test, the in-situ EMR is dried in the drying oven at 75 ℃ for 60 hours, and then crushes and grinds until it can pass through a 150 meshes sieve, and the basic physical characteristics of EMR are shown in Table 3.

Table 1 Physical and mechanical properties of P.I. 42.5R Portland cement

Surface area ($m^2 \cdot kg^{-1}$)	Standard consistency water (%)	Stability	Setting time (min)		Flexural strength (MPa)		Compressive strength (MPa)	
			Initial	Final	3 d	28 d	3 d	28 d
4.2	30.1	Qualified	176	223	5.2	6.3	25.0	42.5

Table 2 Oxide composition of Portland cement

Materials	SiO_2	Al_2O_3	Fe_2O_3	CaO	MgO	SO_3	Na_2O	K_2O	*f*-CaO	LOI
PC	20.08	5.29	3.01	63.41	2.06	2.17	0.32	0.40	0.90	3.6
EMR	34.67	9.01	21.21	5.58	0.61	20.53	0.43	1.58	-	19.58

Table 3 Basic physical properties of EMR

Material	Water content (%)	Specific surface area ($m^2 \cdot g^{-1}$)	Density ($g \cdot cm^{-3}$)	Stacking density ($g \cdot cm^{-3}$)	pH
EMR	31.0±2	4.0±0.1	2.7±0.2	0.9±0.1	6.2±0.2

2.2 Sampling and curing regime

In this study, the main research procedures including the sample preparation, the sample testing and the assessment of environmental implication are presented in Fig. 1. During the preparation of plastic triple molds, the graphite electrode slices (40mm × 50mm × 5mm) with high conductivity and inert with cement were placed into both ends of the molds beforehand and fixed with the hot melt adhesive. The mass ratio of water to cement is always 0.5, and the ratio of cement to EMR ranges from 1:9 to 5:5. The details of test design are presented in Table 4. Cement particles and EMR were blended in a mixing pot for pre-stirring 1 minute, and then adding water for 5 minutes of wet mixing including slow mixing (150 r/min) for 2 minutes and fast mixing (300 r/min) for 3 minutes. After mixing, the cement paste was poured into the plastic molds (40mm×40mm×160mm) and molded by a vibrating table in vibration. Immediately, the surface of the samples was covered by polyethylene film for preventing the water evaporation. The label “DMP-9” means that the pastes with the ratio of cement to EMR is 1:9 cured in the DEC system, and so does the other labels.

Table 4 The parameters of different curing methods for specimens.

Group No.	Label	Curing method	Cement: EMR	Voltage (V)	Curing time (h)	Frequency (Hz)
A1	DMP-9	DEC	1:9	12	8	50
A2	DMP-8	DEC	2:8	12	8	50
A3	DMP-7	DEC	3:7	12	8	50
A4	DMP-6	DEC	4:6	12	8	50
A5	DMP-5	DEC	5:5	12	8	50
A6	DMP-0	DEC	0:10	12	8	50
B1	DMP-8	DEC	2:8	8	8	50
B2	DMP-5	DEC	5:5	8	8	50
C1	DMP-8	DEC	2:8	24	8	50
C2	DMP-5	DEC	5:5	24	8	50
D1	IMP-8	IC	2:8	0	0	0
D2	IMP-7	IC	3:7	0	0	0
D3	IMP-5	IC	5:5	0	0	0

The DEC equipment was independently developed in laboratory as shown in Fig. 2. The whole DEC equipment include controlling, recording and heating module. According to our previous studies (Yang et al., 2021; Ma et al., 2021), the curing time is stated at 8h, and the frequency of alternating current is also fixed at 50 Hz. Different from steam curing and microwave curing, the self-design insulation box and alternative current power supply was used for curing samples in DEC system. Specifically, the cuboid insulation box is prepared by a plastic box, in which the internal aluminum foil sponge patch is adhered to sealing and insulation. In addition, the plastic molds were placed into the heating module immediately after preparing the paste. The DEC regimes employed in this study are exhibited in Fig. 3. The voltage of DEC ranges from 8V to 24V for investigating the effect of DEC voltage on cement hardening. After DEC, all samples were transferred into standard curing room with temperature of 20±2℃ and relative humidity of 95±3% until the demolded operation at 1 day. When the hardened cement pastes were demolded, and they were sequentially cured in the standard curing condition.

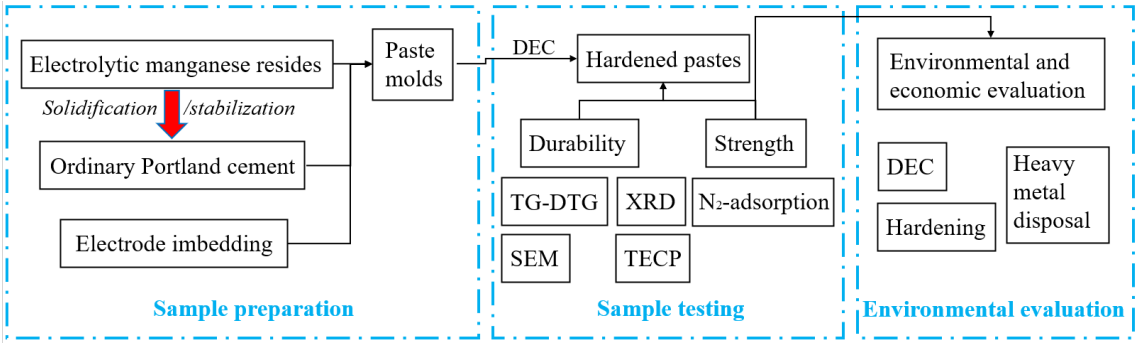

Fig. 1. The overall research procedure of this study

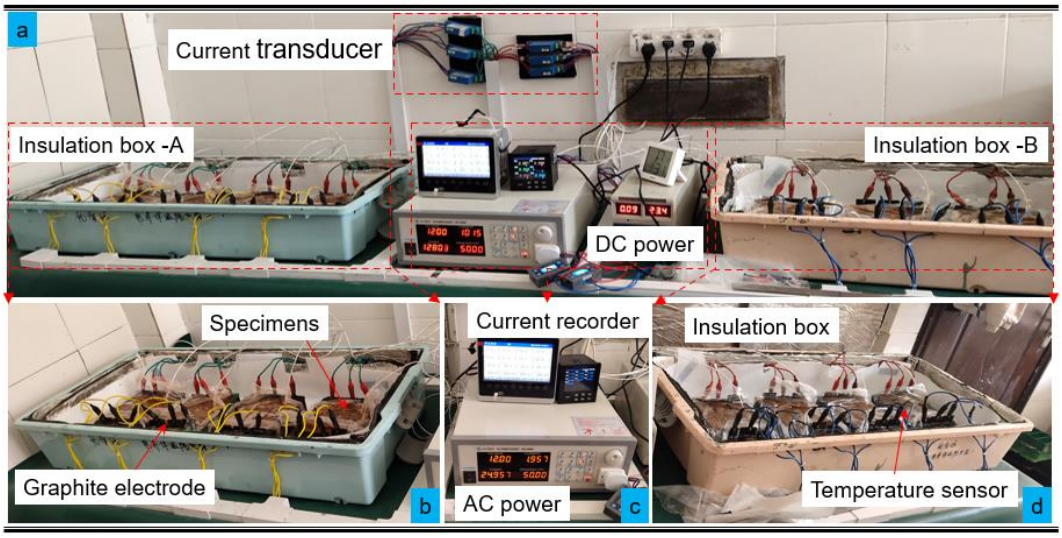

Fig. 2. The equipment for direct electric curing. a) the whole curing system. b) the insulation box-A. c) AC power and recorder. d) the insulation box-B.

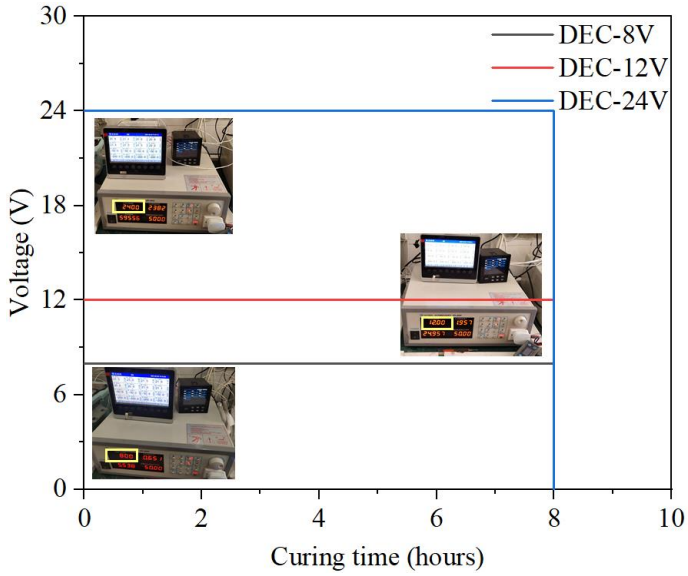

Fig. 3. The DEC regimes used in this study

2.3 Testing methods

When the paste cured to scheduled testing ages, the cured samples were taken out from the standard curing room and left to dry naturally for 3 hours to make surface dry before strength measurements. The flexural strength of paste was conducted firstly with the vertical loading rate of 50 N/s. The broken specimens were collected for further measuring the compressive strength with the loading rate of 2.4 kN/s. In other words, three samples were employed to detect the flexural strength, and then six broken specimens were used to accomplish compressive strength. Thus, the flexural strength data used in next section is the average value of three test results. And the compressive strength results were calculated

from more than four test results after foreclosing the results with bias greater than 15%.

When finishing compressive strength tests, some sheet crushed samples with the size of about 3~5 mm were selected for accomplishing a series of microstructure tests. After sample collecting, all selected samples were immersed into isopropanol solution for terminating cement hydration. The reaction-terminated samples were transferred into vacuum oven for drying at 45±2° C.

Based on the nitrogen adsorption isotherm, the pore size distribution of the blocky samples with the size of 1-2 mm is calculated by the Barrett-Joyner-Halenda (BJH) method (Thommes et al., 2015). Through N_2 adsorption tests, the obtained smallest pore diameter is about 0.5 nm, and the maximal pores diameter achieve about 200 nm.

The capillary water absorption of 28-d paste was measured based on ASTM C1585-20. It is noted that the paste specimens were oven-dried at 60±2° C for at least 72 hours until the mass of samples keeps a constant. The side edges of paste were sealed by paraffin, and the upper half part of specimens was wrapped by combining the preservative film and elastic cord. The weight of oven-dried specimen, paraffin, preservative film and elastic cord is defined as the total mass. The immersion depth of tested sample was controlled at 3 mm at a constant environment (20±2° C, 75±10% RH). At the corresponding test time, the samples were removed from the water tank and then weighed.

The thermogravimetric analysis (TGA) and X-ray diffraction analysis (XRD) were conducted to analyze the effect of DEC on cement hydrated reaction. Similar to the sample preparation process of N_2 adsorption tests, the processes of hydration termination and oven-drying are the indispensable operation. More than 100 mg Samples for XRD and TGA should be ground into powder until it could pass through 100 *u*m sieves. The testing temperature of TGA ranges from 35° C to 1050° C, and the temperature rising rate was set as 10° C/min. The contents of chemical bound water and $Ca(OH)_2$ are calculated by thermo-gravimetry and derivative thermo-gravimetry (TG-DTG) curves. The weight loss of the specimens ranging from 35° C to 550° C is classified as the chemical bound water content. The loss in range of 350~550° C is defined as the $Ca(OH)_2$ content. Based on the TG-DTG curves, the hydration degree of cement paste also can be calculated. CuKα radiation ($\lambda = 0.154$ nm, 40 kV, 50 mA) was conducted during XRD tests via using an X-ray diffractometer with a step width of 2°/min. The measured interval is from 10°to 45°(2θ). The hydration products morphology of paste was observed by a scanning electron microscope (SEM).

The leaching tests of paste were conducted using the horizontal vibration extraction procedure (HJ/T 300-2007; HJ-557-2010; HJ 908-20). The fragmentized samples (5g each) were placed into a plastic pot with a mass ratio of solid to liquid is always 1:20 (100 mL). After vibrating for 16 hours at a frequency of 120 min^{-1} and then sitting for 8 hours, all samples were filtered and stored for accomplishing inductively coupled plasma optical emission spectrometry (ICP-OES) tests. Atomic absorption spectrophotometry inflame was used for determining the concentration of metal ions (HJ 484-2009). NH_4^+-N was measured via Nessler's reagent spectrophotometry method of HJ 535-2009 (Standards, 2009b) and GB/T 205-2000 (Standards, 2000).

In order to analyze the environmental implication of DEC, the carbon dioxide equivalent (CO_2-e) index was employed to evaluate the energy consumption (eq. (1)) (Shi et al., 2019). Previous studies indicated that the CO_2 emission of Portland cement and DEC is 0.73 kg/kg and 2.1 kg/m^3·h, respectively. Due to EMR is classified as a hazardous solid waste and the tested EMR is obtained from the same pitch, the CO_2 emission of EMR is not considered. The economic analysis of DMP and IMP was conducted to investigate the cost saving. The authors introduced the 28-d compressive strength and hazardous compounds for further calculating the expansive index (eq. (2)).

$$EIF = \frac{ECO_2\text{-e}}{F_{c28}} \quad (1)$$

EIF with the unit of kg/MPa • m^3 is the modified CO_2-e index which can compare the CO_2 emission levels of cement-base materials with different strengths. And f_{c28} is the 28-d compressive strength.

$$CSF = \frac{\sum C_i}{F_{c28}} \quad (2)$$

CSF with the unit of RMB/MPa • m^3 is the modified cost index which can compare the cost levels of cement-base materials with different strengths.

3. Results

3.1 Effects of Cement/EMR on mechanical properties of cement pastes

The measured strength values of cement pastes with different EMR doses in the 12V-DEC are presented in Fig. 4 and Fig. 5. It is observed that the increase in cement equivalent can increase the 3-d compressive and flexural strength. The 3-d compressive and flexural strength values of pastes DMP-9 are 0.84 MPa and 0.46 MPa, respectively. As the ratio of cement equivalent to EMR increases from

10% to 50%, the 3-day compressive and flexural strengths achieve 12.59 MPa and 2.38 MPa, about 14.98 and 5.17 times than those of paste DMP-9. In addition, the 3-day compressive and flexural strengths of paste DMP-0 are significantly higher than those of paste with EMR. This implies that the increase in the ratio of cement equivalent to EMR could improve the mechanical properties judged by only 3-day strength.

The strengths increase with lengthening the curing ages, but the improvement from 3-d to 28-d for specimens with high EMR dosing (especially in 90% and 80%) are much lower. When the cement equivalent is higher than 30%, the strength increments from 3-d to 28-d are remarkable. The 28-d compressive strength values of pastes DMP-9 and DMP-8 are 2.25 MPa and 8.29 MPa, about 2.68 and 6.69 times than their 3-d compressive strength. And the maximal 28-d compressive and flexural strength of the paste with EMR appear in paste DMP-5, which reach 24.94 MPa and 4.31 MPa, respectively. Compared with the pastes without EMR, the 28-d compressive and flexural strength of pastes DMP-5 reach 57.80% and 51.87% of those of paste DMP-0, respectively. Although paste DMP-5 does not have the highest 3-d strength in all samples, but the suitable strength and the low economic cost indicate that the suitable cement to EMR ratio exists the optimal situation.

The above strength results can be explained by the cement hardening in DEC and the low-activity of EMR. In 12V-DEC system, the electric field can accelerate the ions moving in cement paste, resulting in the improvement in the probability of collision and temperature rising. The introduced EMR can increase the ion concentration in DEC since EMR is acid leaching residue rich in soluble substances. However, the EMR cured in DEC doses not significant increase strength due to its low-activity. The increase in cement equivalent can increase strength because of the cement hydration. The improvement of ion concentration in DEC acts on accelerator to increase the hydration products.

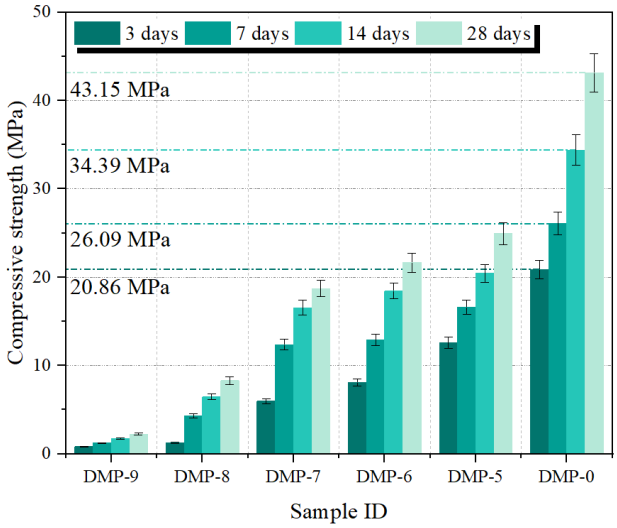

Fig. 4. (a) Compressive strength and (b) flexural strength at different curing ages of 12V-DEC cured cement pastes

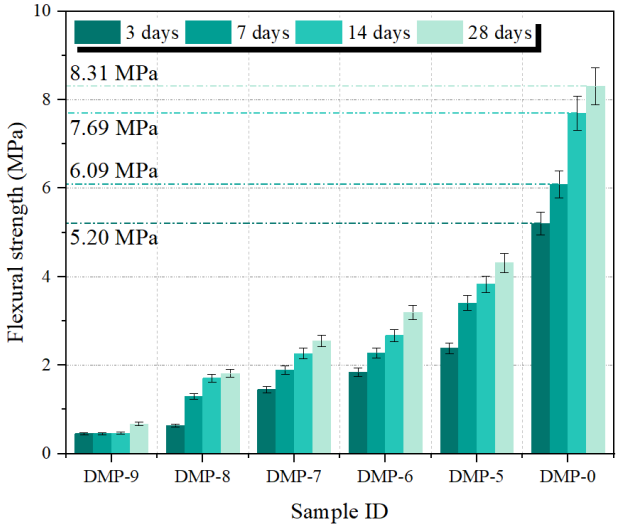

3.2 Effects of curing voltage on mechanical properties of cement pastes

The effects of curing voltage (8V, 12V and 24V) on compressive and flexural strength of pastes DMP-8 and DMP-5 are exhibited in Fig. 6 and Fig. 7. It indicates that the increase in curing voltage does not improve the 3-d and 7-d compressive and flexural strength of paste DMP-8, but can significant enhance the 3-d and 7-d strength of paste DMP-5. Not only that, the increase in cement equivalent can improve cement hardening effect, the increased voltage can enhance the ionic driving force. The 3-d compressive and flexural strength values of paste DMP-5 in 24V-DEC are 14.07 MPa and 2.52 MPa, respectively. In other words, as the curing voltage increases from 12V to 24V, the 3-d compressive and flexural strengths increase 1.12 and 1.06 times than those of paste DMP-5. This means that the increase in curing voltage can improve the mechanical properties of paste with high cement equivalent (i.e.,

DMP-5).

As the curing ages lengthening to 14-d and 28-d, the compressive and flexural strengths of pastes cured in DEC with higher voltage increase significantly. In terms of curing voltage increasing from 8V to 12V, the 28-d compressive strengths of paste DMP-5 are 21.67 MPa and 24.94 MPa, about 2.42 and 1.98 times than of 3-d values. When DEC voltage further increases to 24V, the 28-d compressive and flexural strengths of paste DMP-5 are 28.45 MPa and 5.91 MPa, about 2.02 and 2.35 times than of 3-d. And the maximal 28-d compressive and flexural strengths of paste DMP-5 appear in 24V-DEC, which is attributed that the enhanced voltage can provide a stronger ion collision and higher thermal effect. Compared with the pastes cured in different DEC voltages, the 28-d compressive strength of pastes DMP-5 cured in 24V-DEC reach 114.1% and 131.3% of that cured in 12V and 8V, respectively.

In a word, DEC in 8 hours can accelerate ion migration and then increase the probability of ion collision (Yang et al., 2021). The release from Joule heat leads to a temperature rising, resulting in thermal effect which promote the cement hydration. Thus, the strength of paste with EMR can improve in DEC, and the increase in DEC voltage can boost the sample strengths.

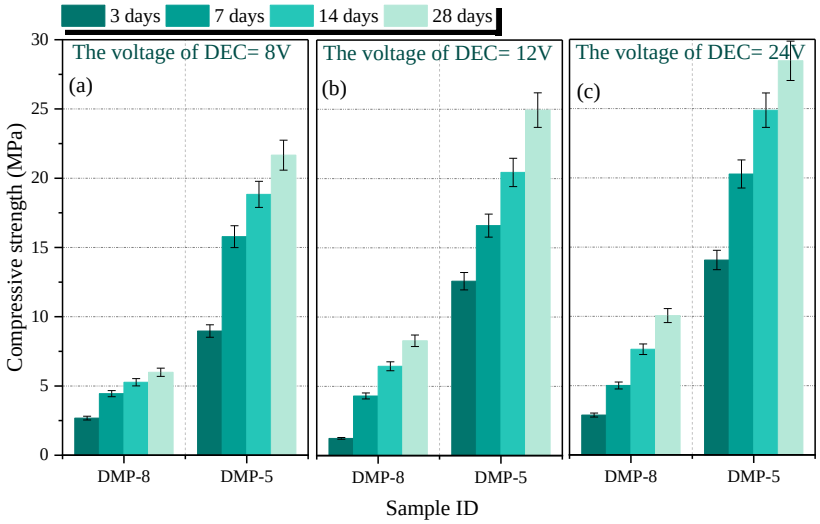

Fig. 5. (a) Compressive strength and (b) flexural strength at different curing ages of cement pastes in DEC with different voltages

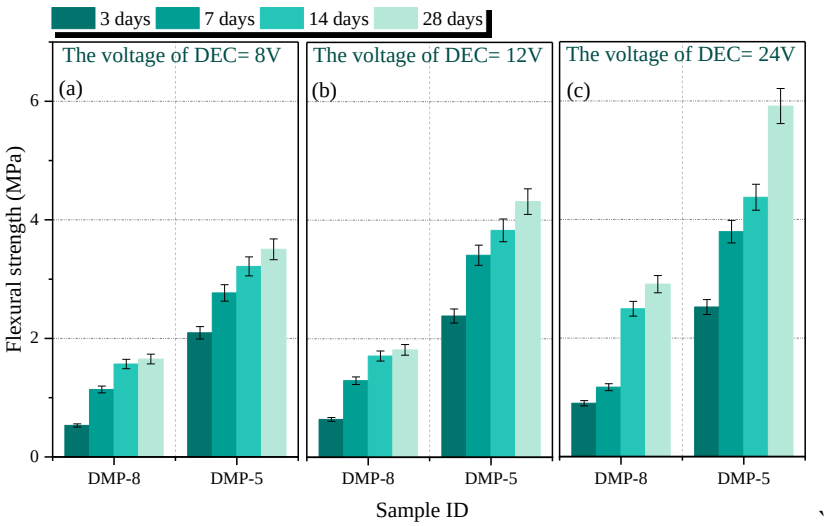

294

295 **3.3 Effects of DEC on mechanical properties of cement pastes**

296 Based on the contrastive analysis, the effects of 12V-DEC and IC on compressive and flexural
297 strength of pastes with different cement equivalents are presented in Fig. 8 and Fig. 9. It shows that
298 the compressive and flexural strength values of cement pastes with a higher cement equivalent can
299 significantly increase with lengthening curing ages in 12V-DEC and IC. It also indicates that pastes
300 cured in DEC can increase the strength values with respect to that cured in IC.

301 In comparation with IMP-8, the 28-d compressive strength of paste DMP-8 can slightly increase,
302 and the increasement is about 0.46 MPa. Also, the increasement in 28-d compressive strength of DMP-
303 7 and DMP-5 is 1.99 MPa and 5.33 MPa with respect to IMP-7 and IMP-5, respectively. The flexural
304 strength values of pastes cured in 12V-DEC are also higher than that cured in IC, i.e., the 28-d flexural
305 strength of paste DMP-5 is about 162.7% with respect to IMP-5. The above phenomenon further
306 exhibits pastes cured in DEC can improve the mechanical properties. The increasement increase with
307 the increase of cement equivalent, which is attributed to the improvement of cement hydration.

308 The underlying reason for improving the strength of pastes in DEC can be classified into two points.
309 One is that DEC forms a driving force accelerating the ions migration and collision, and then promoting
310 the cement hydration process. The other is that the voltage of DEC can release heat due to the Joule
311 thermal effect, which is also contributed to strength development.

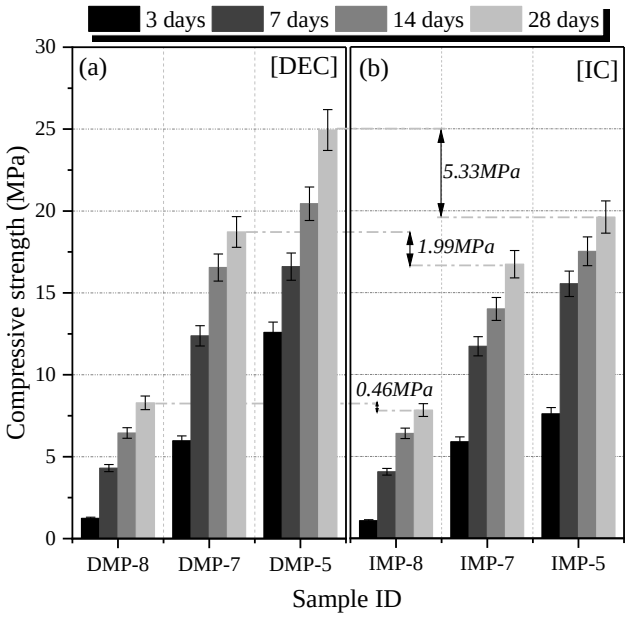

312

313 **Fig. 6. (a)** Compressive strength and (b) flexural strength at different curing ages of pastes in (a)12V-
314 DEC and (b) IC.

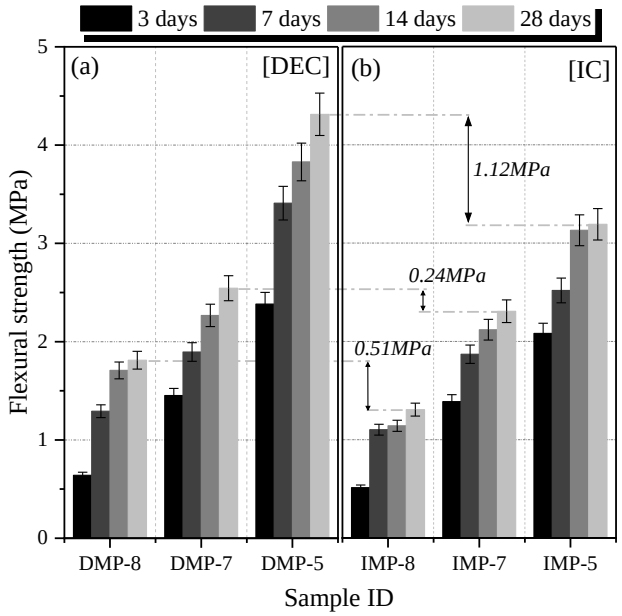

315

316 **3.4 Evolution in pore structure**

317 3.4.1 N_2 Adsorption-desorption chrematistics

318 The low-temperature nitrogen adsorption test was employed to investigate the pore characterization
319 of cement-EMR pastes in DEC with different voltages. The adsorption and desorption curve of three
320 selected 28-d pastes cured in 12V-DEC are presented in Fig. 10. It exhibits that all the selected 28-d
321 specimens have a significant hysteresis loop due to the capillary condensation, which means the

complex pore structure is existed in all the pastes cured in 12V-DEC. According to the morphology of hysteresis loop, the pastes DMP-8 and DMP-5 approach the type-H3, which also indicates that the pore structure are many slit holes formed by the lamellar particle accumulation. The hysteresis loop morphology of paste DMP-0 is between type-H3 and type-H2. It is explained that accumulation of homogeneous ions happens in DMP-0.

Based on Fig.10, the whole adsorption volume decreases with increasing cement to EMR ratio judged by the three selected pastes. The adsorption volume of pastes DMP-8, DMP-5 and DMP-0 is 16.49 cc • g^{-1}, 10.78 cc • $g^{-1}$and 7.17 cc • g^{-1}, respectively. The increase in cement equivalent can significantly decreases the whole pore volume of pastes, meaning that higher cement equivalent produces more cement hydration products to fill paste holes. Fig. 10 indicates that the most adsorption volume main produces in high P/P_0 (0.8~1.0) and less volume produces in low P/P_0 (0 ~0.3), implying that there are maximal micropore existed in pastes cured in DEC.

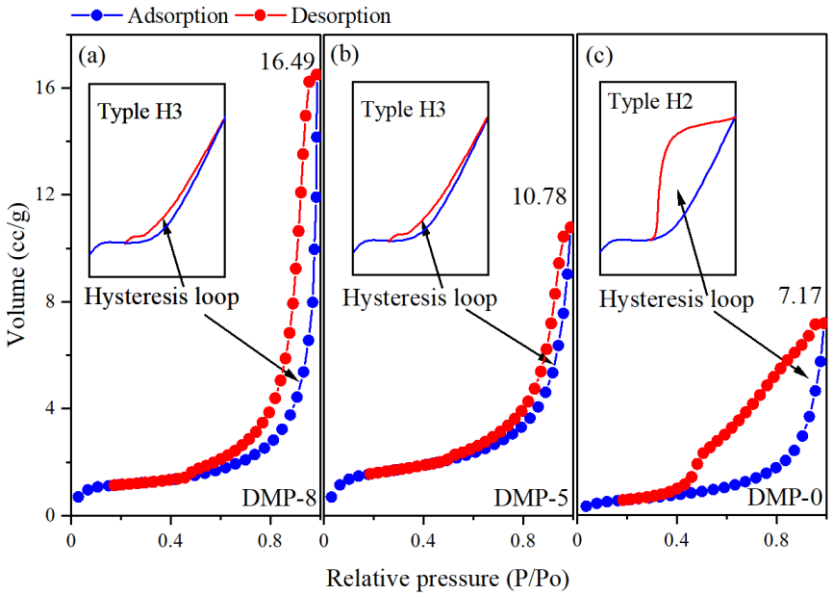

Fig. 10. Adsorption-desorption curve of three selected 28-d pastes (a) DMP-8, (b) DMP-5 and (c) DMP-0 cured in 12V-DEC

The adsorption and desorption curves of 28-d paste DMP-5 cured in different DEC voltages are exhibited in Fig.11. The pore adsorption volume of three selected pastes decreases with the increase of DEC voltage. As DEC voltage increases from 8V to 12V, the decrement in total pore volume of paste DMP-5 is 0.74 cc • g^{-1}. The decrement in total pore volume is 1.34 cc • g^{-1} while the DEC voltage increases from 12V to 24V. The increase in DEC voltage does not alter the morphology of hysteresis

loop and the pore structure distribution. The adsorption and desorption curves of 28-d pastes DMP-8 and DMP-5 cured in 12V-DEC and IC are presented in Fig. 12. The pore volume of pastes cured in IC are higher than that cured in 12V-DEC, which indicates that paste cured in DEC can promote the decrease in total pore volume. The results also can further explain the strength enhancement in DEC. The similar hysteresis loop means the pore structure and distribution of pastes cured in DEC does not happen significant change with respect to IC.

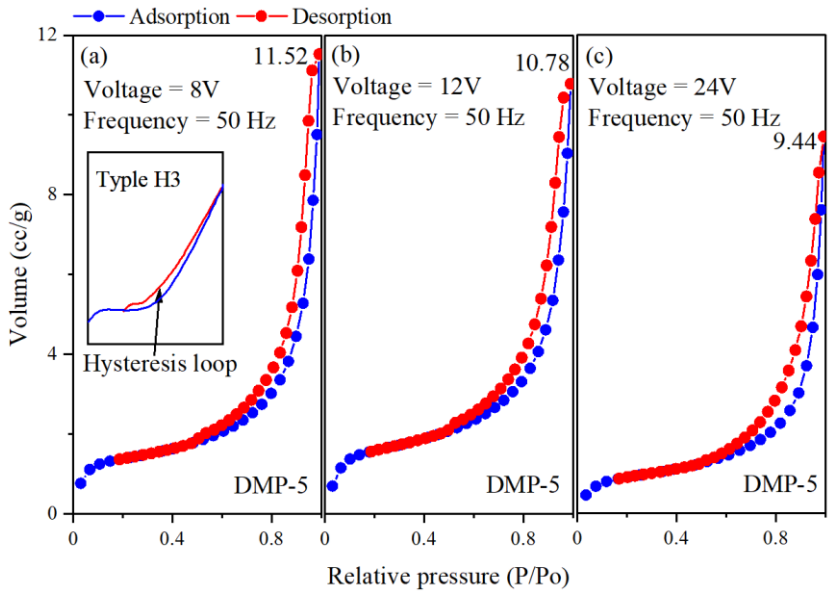

Fig. 11. N_2-Adsorption-desorption curve of 28-d pastes DMP-5 cured in different voltages (a) 8V (b) 12V and (c) 24V

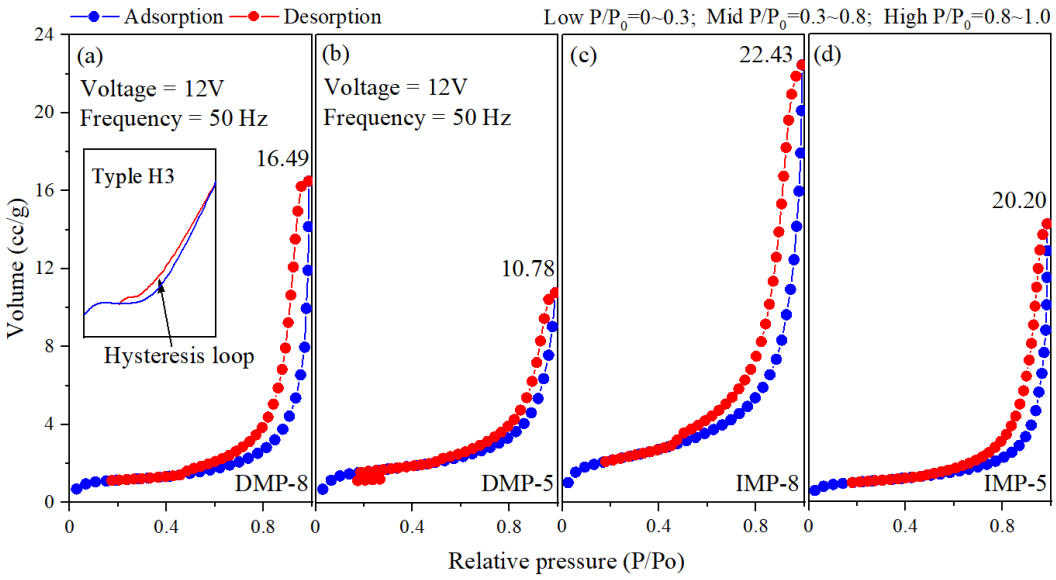

Fig. 12. N_2-Adsorption-desorption curve of 28-d pastes cured in 12V-DEC (a) DMP-8, (b) DMP-5 and IC (c) IMP-8 and (d) IMP-5.

3.4.2 Pore volume and size distribution

The sum pore volume and pore size distribution of the most probable pore of 28-d mixtures are exhibited in Fig. 13. The pore size distribution of all tested pastes main consists of two peaks classifying into the mesopores interval. In 12V-DEC (Fig. 13a), the cumulative pore volume increases with increasing the cement to EMR ratio. The sum pore volume of paste DMP-5 cured in 12V is 0.27 cc • g^{-1}, accounting for 49.1% of paste DMP-8. The above result strongly verifies the mechanical properties of relevant pastes. The sum pore volume of paste cured in 8V has the similar value to that cured in 12V, but the macropores of paste cured in 8V is higher than that in 12V, as shown in Fig.13b. The sum pore volume can further decrease with the increase of DEC voltage from 12V to 24V. The sum pore volume of paste cured in 24V is 0.19 cc • g^{-1}, which accounting for 70.4% of paste DMP-5 cured in 12V. The characteristics of the curves of the pore distribution present significant difference. In other words, a broad peak is observed in the curve of pastes DEC-5 cured in 24V, and the peaks in other two mixtures change sharply. The significant decrease in sum pore volume of pastes cured in DEC with respect to IC curing. Based on Fig. 13c, the sum pore volume of the paste IMP-5 is 0.68 cc • g^{-1}, about 2.5 times than pastes after 12V-DEC. It means that pastes after DEC can optimize the pore size distribution and decrease the sum pore volume. In addition, the probably essential reason is that DEC can promote cement hydration and reaction between C_3A and EMR. And then the formed hydration products can fill paste pore, adjusting pore structure and improving strength.

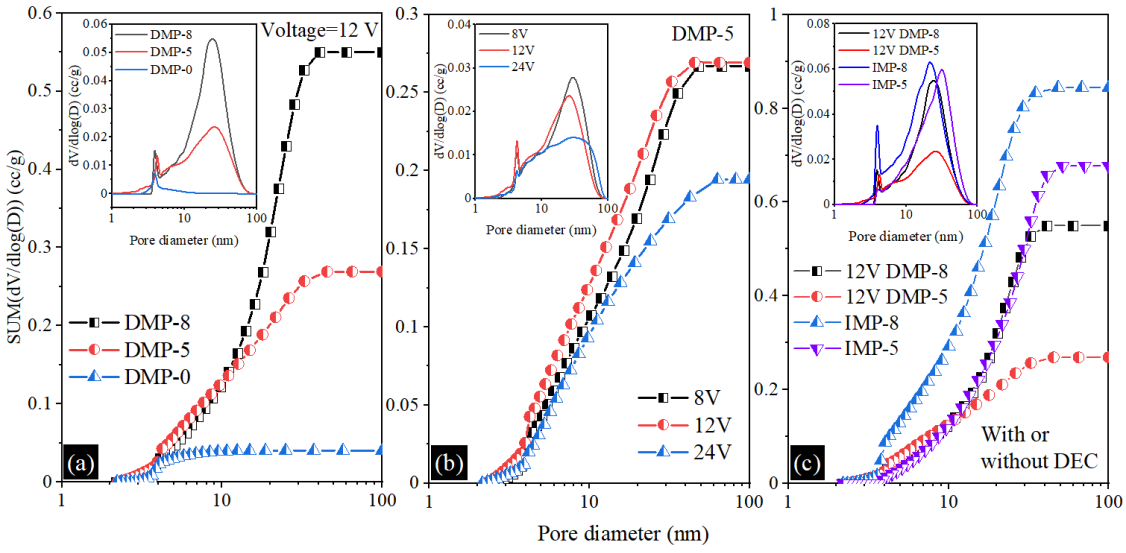

Fig. 13. Sum pore volume and pore size distribution of 28-d pastes (a) 12V-DEC, (b) different DEC voltages and (c) IC.

According to the International Union of Pure and Applied Chemistry (IUPAC), pores are classified into three types: macropores (≥50 nm), mesopores (2-50 nm), and micropores (≤2 nm), and the pore structure and volume percentage is presented in Fig.14 [24]. In 12V-DEC, the total porosity of pastes DMP-8 is much higher than the other two mixtures in both macropores and mesopores. This also corresponds to the tendency exhibited in strength. There is a remarkable difference in the distribution of the most probable pore of three pastes cured in 12V-DEC. In addition, paste DMP-8 has the highest proportion of harmful pores than the other two pastes. This is related to the equivalent of cement, and the paste DMP-8 has the lowest cement and highest EMR. Moreover, the increase in DEC voltage can decrease the macropores volume, and the pastes DMP-5 cured in 24V has the lowest harmful pores than the other two pastes. It implies that the DEC with high voltage has a significant contribution to change the pore structure due to the acceleration in cement hydration. Different from paste cured in DEC, pastes cured in IC has the higher macropores and mesopores. From Fig. 14, the paste IMP-5 has a remarkable increase with respect to paste DMP-5 in both pore diameter. The above results can be explained by the improvement of pore structure. A remarkable decrease in the proportion of mesopores is observed in Fig.13 and Fig. 14, or a large number of macropores transform into mesopores. This is possibly because the continuous growth and diffusion of hydration products fill in the mesopores gradually.

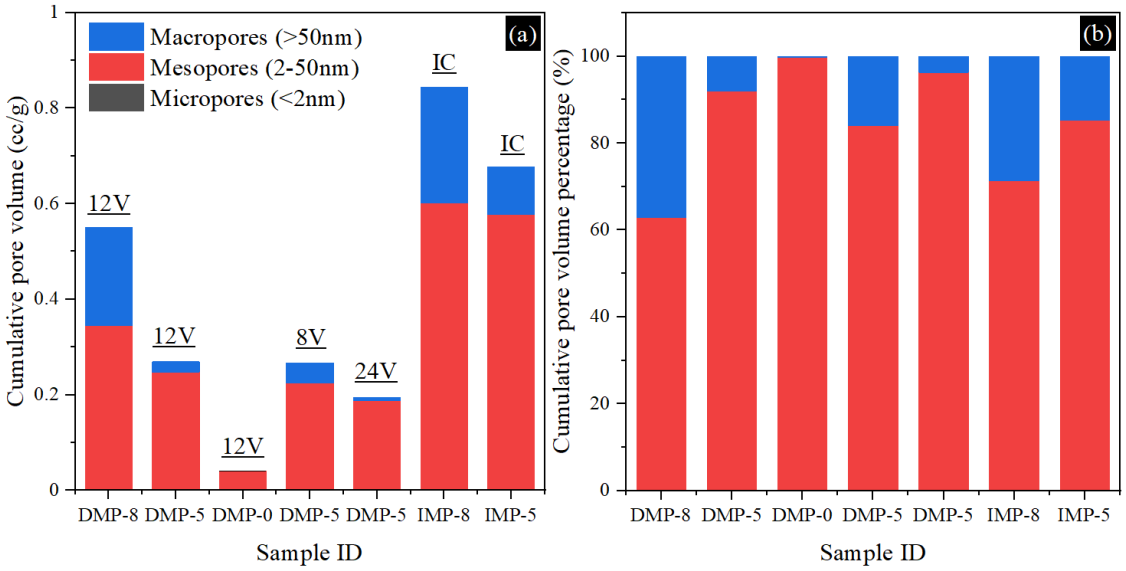

Fig. 14. Pore structure (a) cumulative pore volume and (b) cumulative volume percentage of the selected 28-d pastes

3.5 Capillary water absorption

The results of capillary water absorption of all selected 28-d pastes are presented in Fig. 15. The cumulative volume of water permeation increases with the increasing square root of time. The cumulative volume of all selected pastes can be divided into two stages based on the different rising rate. Based on capillary pressure from cement paste, water migration from the bottom into cement pastes occurs immediately after the bottom of samples immersing into water, and then the speed of initial water migration is higher than the latter one. It is probable explained by the water migration in later stage occurs significantly in more smaller pores, as reported in previous studies (Bi et al., 2020). Meanwhile, the relationship between the water permeation volume and square root of time could be calculated by the under-mentioned equation, which also exhibited in Fig.15.

$$i=k\times\sqrt{t}+l \qquad (3)$$

where i (mm) stands for the cumulative volume of water permeation, k (mm • $s^{-1/2}$) represents the migration rate of water into cement pastes and l is a constant value gained from the intercept of the fitted curves. The k and l values obtained from fitted curves are exhibited in Table 5. The slope of the first-stage of each specimen is much higher than the second-stage one. Based on the Fig.15, DEC and cement equivalent have a significant influence on the capillary water absorption, which can be expressed from the following aspects. Firstly, the increase in cement equivalent can decrease the final cumulative volume of water permeation in both two stages. In all the tested paste with EMR, pastes DMP-5 has the highest i value, and the lowest i value exists in paste DMP-9. Secondly, the increase in DEC voltage also decreases the final cumulative volume of water permeation in both two stages. Paste DMP-5 cured in 24V has the highest i value, and the lowest one happens in paste cured in 8V. Thirdly, the final cumulative water permeation volume of pastes cured in DEC is lower than that cured in IC. The same tendency of cement to EMR ratio existed in paste cured in IC. In addition, the k value of all pastes has the same tendency with i value in different curing conditions and cement equivalents.

The relationship between the pore structure and capillary water absorption is attempted to establish for investigating the possible mechanism for the above phenomena (Jia et al., 2016; Pan et al., 2017). Previous studies believed that the capillary water adsorption in first-stage is attributed from the macropores with the size ranging from 200nm to 1000nm, and the number of pores smaller than 200 nm may be related to the second-stage capillary water absorption. Thus, the proportions of the tested

pores in the pastes cured in IC are much higher than that cured in DEC based on results of water migration rate. The proportions of pores in the pastes cured in high-voltage DEC and high cement equivalent are higher than that in low-voltage and low cement equivalent. This not only complements the nitrogen adsorption test results, but also validates with strength development in all selected pastes.

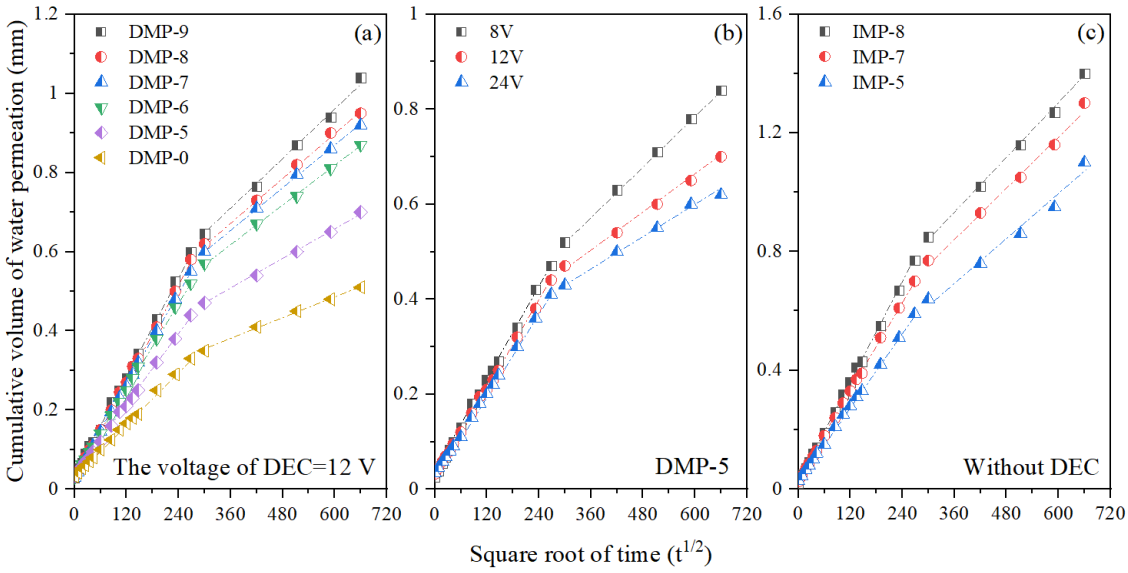

Fig. 15. Capillary water absorption (a) pastes with different cement equivalent, (b) pastes with different DEC voltages and (c) pastes cured in IC and the two-stage fitted curves.

Table 5 Parameters data of results obtained from the fitted curves

Pastes. ID	First stage			Second stage		
	k (10^{-2})	l (10^{-2})	R^2	k (10^{-2})	l (10^{-2})	R^2
12V-DMP-9	0.211	3.237	0.98	0.108	31.638	0.99
12V-DMP-8	0.205	2.789	0.99	0.093	34.043	0.99
12V-DMP-7	0.195	2.786	0.98	0.089	33.566	0.98
12V-DMP-6	0.184	3.030	0.97	0.083	32.020	0.99
12V-DMP-5	0.151	3.094	0.98	0.064	27.549	0.99
12V-DMP-0	0.111	3.276	0.96	0.044	22.145	0.96
8V-DMP-5	0.167	2.770	0.99	0.089	25.515	0.97
24V-DMP-5	0.141	3.187	0.99	0.054	27.066	0.98
0V-IMP-8	0.279	2.400	0.96	0.0151	39.053	0.95
0V-IMP-7	0.253	2.509	0.99	0.0144	32.839	0.97
0V-IMP-5	0.208	2.927	0.97	0.0123	25.255	0.99

3.6 Mineralogical characterization

3.6.1 TG-DTG results

The TG-DTG curves of three selected 28-d pastes cured in 12V-DEC are presented in Fig. 16. Based on the TG-DTG curve, the main weight loss happens in three different temperature intervals. In the first temperature intervals, the dehydration process of C-S-H gels and ettringite (AFt) accomplished within 200° C. In the second temperature intervals, the decomposition of Portlandite (CH) happened in 350~500° C. At the last intervals, the decomposition of muscovite and recrystallization of mineral

phase obtained from EMR occurred in the above 750° C. However, it is difficult to directly distinguish the amount for different types of hydration products just judged by the TG-DTG results. For this reason, the amount of CH can reflect the cement hydration to some extent (Gaviria et al., 2018). Thus, pastes DMP-0 have the highest degree of cement hydration, followed by pastes DMP-5, and followed by pastes DMP-8. This is consistent with the tendency in compressive strength.

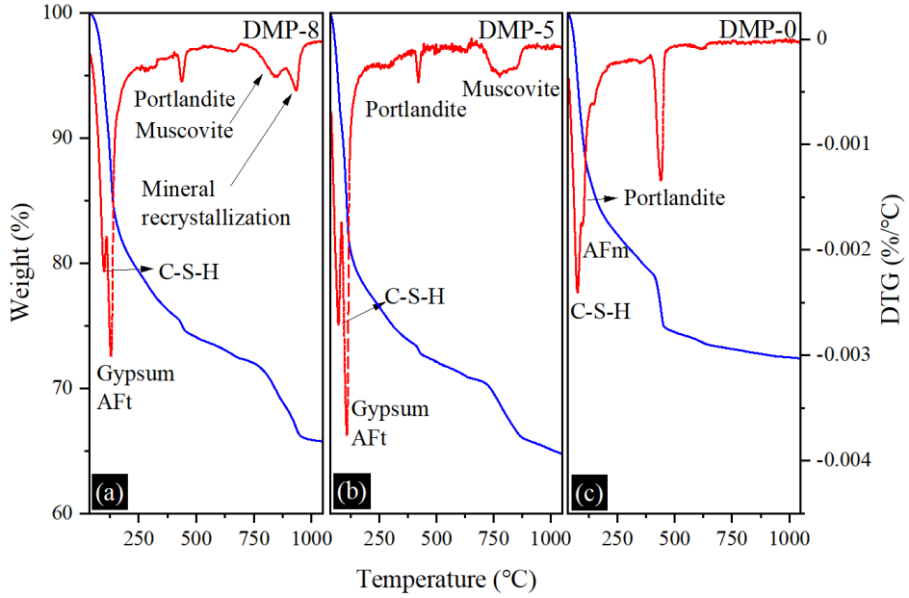

Fig. 16. TG-DTG curves of 28-d pastes (a) DMP-8, (b) DMP-5 and (c) DMP-0 cured in 12V

The TG-DTG curves of three selected 28-d pastes cured in DEC with different voltages are exhibited in Fig. 17. The main weight loss also occurs three different temperature intervals with respect to Fig.16. As the DEC voltage rising from 8V to 12V, the dehydration amount of C-S-H gels and ettringite (AFt) is significant increase, but the amount of CH does not change remarkable. And the same tendency presented when the voltage further rising to 24V. In addition, the TG-DTG curves of the selected 28-d pastes cured in IC are exhibited in Fig. 18. Compared with the Fig.16 and Fig.18, it indicates that pastes cured in DEC can promote the cement hydration than that cured in IC based on the variations in CH content. The same tendency does not change with changing the cement equivalent.

In conclusion, in comparison to IC, cement pastes cured in DEC can promote cement hydration process according to the TG-DTG results. The increase in DEC voltage can steady the improvement effect but not further boosting. In addition, the weight loss occurs significantly within 200° C due to the EMR rich in hydrated gypsum. The gypsum reacts with C_3A provided from cement to produce ettringite also the other reason for high weight loss. The about results can be further verified in next

section.

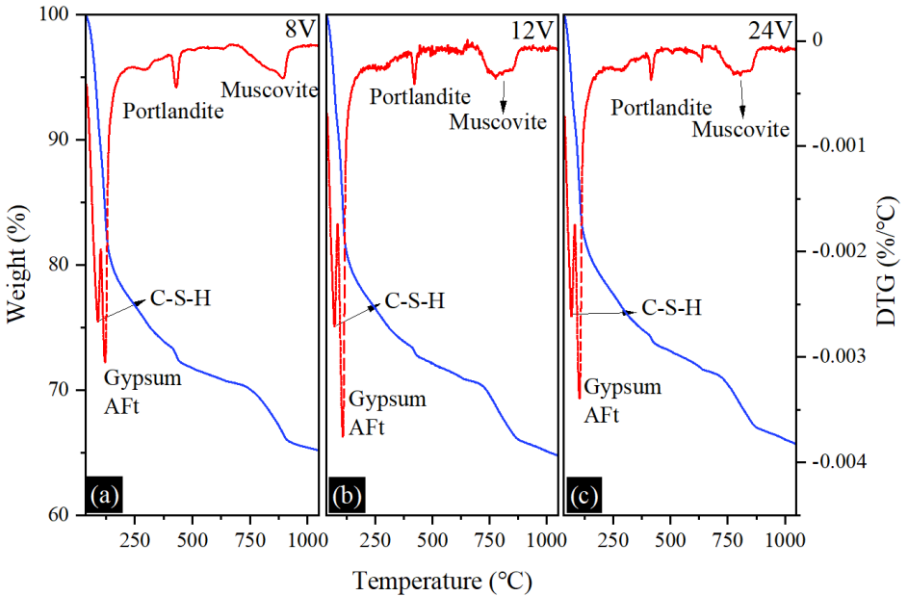

Fig. 17. TG-DTG curves of 28-d pastes DMP-5 cured in DEC with different voltages (a) 8V, (b) 12V and (c) 24V

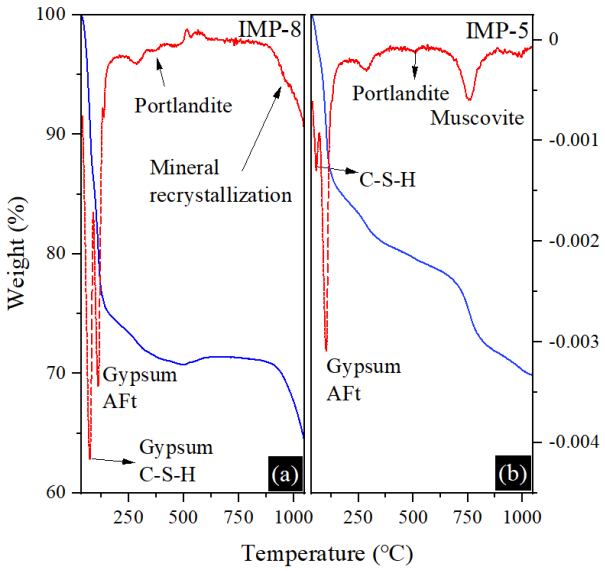

Fig. 18. TG-DTG curves of 28-d pastes (a) DMP-8, (b) DMP-5 cured in IC

3.6.2 XRD results

The XRD patterns of the selected 28-d pastes are shown in Fig. 19. All pastes cured in DEC does not change the types of hydration products with respect to IC. The mineral compositions of all formed cement pastes consist of ettringite, AFm, portlandite and C-S-H gel (tested by TG-DTG). Meanwhile, the other mineral phases main include unreacted cement clinker. The intensity of ettringite peaks of pastes DMP-8 and IMP-8 are higher than those of pastes DMP-5 and IMP-5, which is related to the

increase of gypsum in EMR. In terms of peak intensity of unreacted cement clinker, the application of DEC and the increasement in DEC voltage can promote the cement hydration judged by the decreasing intensity. In addition, the peak intensity of portlandite and ettringite of paste DMP-5 cured in 24V is much higher than that cured in 8V and 12V after increasing DEC voltage. It also implies that DEC with high voltage accelerates the cement hydration. The above results are consistent with the strength. This also indicates that the boosted ettringite formation occurs in cement paste after introducing DEC and amplifying the DEC voltage (Yang et al., 2021). The possible reason is that the experience temperature during EDC is higher than IC, which further analysis in next section. In addition, the transformation of cement hydration products is related to the corresponding proportion of pores.

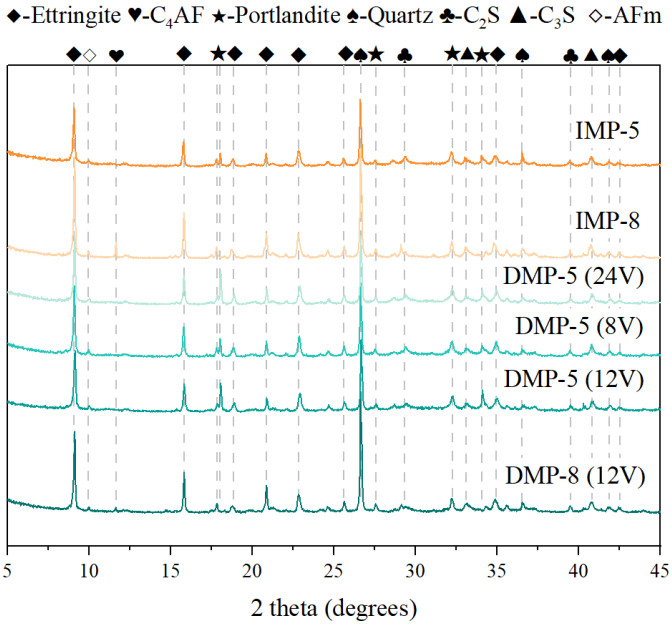

Fig. 19. XRD patterns of 28-d pastes cured in DEC (8V, 12V and 24V) and IC

3.7 Assessment of CO_2-e and economic analysis of EMR indurated in cement pastes

The total CO_2-e values of the pastes cured in DEC and IC are presented in Table 6. Cement pastes cooperating with EMR can decrease the CO_2-e. Through introducing 28-d compressive strength, the CO_2-e per MPa (EIF) and cost per MPa (CIF) of cement-based materials can reflect their real environmental impacts and economic analysis, respectively. In the calculation about EIF, the CO_2-e of DEC can be obtained from lab experiments. In our previous studies, the value was calculated as 2.1 $kg/m^3 \cdot h$ in 18V. According to power conversion and detect by lab, the CO_2-e change with the voltage squared. Thus, the CO_2-e of DEC in 8V, 12V and 24V is 0.415, 0.933 and 3.73 $kg/m^3 \cdot h$, respectively. Because other emission parameters are basically the same, the calculation is no longer carried out.

In terms of calculating CIF, the price of OPC and water is 450 and 4.1 RMB/t, and the density of OPC is 1.95 g/cm^3. ENR as hazardous solid waste can be obtained without excessive economic expenditure and the CO_2-e of stockpiled EMR can be classified as zero-emission for reasonable calculation. The calculated *EIF* and *CIF* values are presented in Table 6. Significant difference in cement equivalent is observed in Table 6. The *EIF* and *CIF* values decrease as EMR reducing from 90% to 50%, and the decrement is intimately related to the increase in strength. The ratio of cement to EMR is higher than 3:7, the *EIF* and *CIF* values of pastes cured in DEC has the lower value. In addition, the *EIF* and *CIF* values of pastes DMP-5 cured in 12V-DEC exhibit the lowest values with respect to cured in other voltage. The paste DMP-5 cured in 12V has the lower *EIF* and *CIF* values than that cured in IC. When the CO_2 emission, cost and requirement of strength is considered together, DEC is the most effective and environmentally friendly method for promoting cement-EMR materials, which can further realize the clean and high-efficiency disposal of hazardous solid waste by improving the mechanical properties.

Table 6 Environmental evaluation and economic evaluation of pastes

Pastes. ID	Environmental evaluation		Economic evaluation	
	CO_2-e(kg • m^{-3})	*EIF(kg • MPa^{-1}·m^{-3})*	*Cost (RMB • m^{-3})*	*CIF(RMB • MPa^{-1}·m^{-3})*
12V-DMP-9	17.555	7.82	24.127	10.747
12V-DMP-8	31.79	3.834	47.204	5.694
12V-DMP-7	46.025	2.458	70.281	3.754
12V-DMP-6	60.26	2.918	93.358	4.521
12V-DMP-5	74.495	2.987	116.435	4.668
12V-DMP-0	145.67	3.376	231.82	5.373
8V-DMP-5	78.639	3.63	116.435	5.374
24V-DMP-5	101.015	3.55	116.435	4.092
0V-IMP-8	28.47	3.635	47.204	6.028
0V-IMP-7	42.705	2.552	70.281	4.199
0V-IMP-5	71.175	3.629	116.435	5.936

3.8 Analysis of leaching tests

Mn^{2+} and NH_4^+-N are the hazardous components of most concern in DMP and IMP. Previous studies have shown that cement-based materials are capable of achieving solidification and stabilization of heavy metals. To ensure the safety of EMR utilization, the toxicity characteristic leaching procedure (TCLP) was used to determine the leaching concentration of cement-EMR paste cured in DEC and IC. The leaching results of Mn^{2+} and NH_4^+-N in 3-d and 28-d pastes are shown in Table 7. It indicates that the leaching amount of Mn^{2+} and NH_4^+-N gradually decrease with the cement equivalent. The leaching amount of Mn^{2+} and NH_4^+-N of pastes cured in IC is slightly higher than that cured in DEC. And the

decrease in the leaching amount of Mn^{2+} and NH_4^+-N as the DEC voltage increase. This tendency is consistent with results presented in pore structure and strength development. It is noted that the leaching of Mn^{2+} and NH_4^+-N from 3-d pastes still exceeds the limit of national standard (GB 8978-1996), which is attributed by the high dosing EMR and low cement equivalent. In other words, cement hardening is not significant at early-age cement solidification, but the 28-d results showed that Mn^{2+} and NH_4^+-N in were no longer a serious problem. The leaching of Mn^{2+} of the 28-d pastes with high cement equivalent (>20%) were in accordance with the leaching national standards (GB 8978-1996).Meanwhile, the leaching of NH_4^+-N of all 28-d samples were in accordance with the leaching national standards (GB 8978-1996).

Table 7. Leaching concentrations of EMR-blended mortar using the TCLP

Samples		12V						DMP-5		Without DEC			GB
		DMP9	DMP8	DMP7	DMP6	DMP5	DMP0	8V	24V	IMP8	IMP7	IMP5	limits
3-d	Mn	105.2	85.5	74.2	63.1	50.1	0.5	57.2	35.1	95.2	81.5	60.2	5.0
	NH_4^+-N	47.2	41.5	37.4	35.7	33.1	0.2	34.5	31.6	45.8	43.7	36.3	25.0
28-d	Mn	10.7	7.4	4.9	4.7	3.2	ND	3.7	2.1	9.4	8.3	5.5	5.0
	NH_4^+-N	7.5	6.2	5.4	5.1	2.4	0.1	2.7	2.3	7.1	5.8	4.1	25.0

4. Discussion

4.1 Thermal effects of DEC

The thermal effects of DEC on pastes with different cement equivalents cured in 12V are exhibited in Fig. 20. The calculated differential area is used for investigating the thermal effects of DEC. As the above-mentioned results, the application of DEC can promote cement hydration and optimize pore structure. Combination with previous studies, the temperature rising produced from DEC is the main difference with respect to IC. Based on Fig. 20a, the differential area significant increase with rising cement equivalent. It implies that the introduction of DEC can promote cement hydration. The differential area of pastes DMP-5 is 13184.25, about 75.3% of paste DMP-0. This is also related to the temperature fluctuation as shown in Fig.20b. The application of DEC accelerates the cement hydration through releasing heating. The interior temperature value of paste increase with aggrandizing cement dosing, and the interior temperature of pastes DMP-0 and DMP-5 are 48.675℃ and 32.775℃, respectively. The relationships among compressive strength, EMR dosing and maximum heating are presented in Fig. 20c. It indicates that the 3-d and 28-d compressive strengths has a good linear relationship with heating, and there is a remarkable linear fitting between heating and EMR dosing. The above-mentioned results are contributed by the improvement of 12V-DEC and the reinforcement

of cement hardening, which further verify that the DEC can promote the cement hydration by thermal effects.

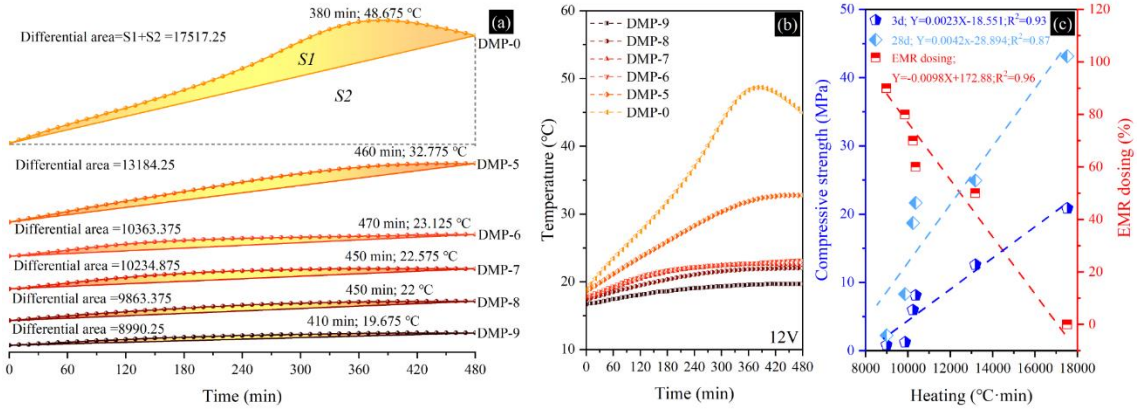

Fig. 20. Thermal effects of DEC on pastes cured in 12V (a) differential area, (b) temperature curves and (c) relationship between compressive strength and heating

The thermal effects of DEC with different voltages and IC on pastes DMP-8 and DMP-5 are presented in Fig. 21. The differential area significant increase with increasing DEC voltages. It implies that the introduction of DEC with high voltage can significantly promote cement hydration. The differential area of pastes DMP-5 cured in 24V is 18021.125, about 1.6 times than that cured in 8V. This is also related to the temperature fluctuation as shown in Fig.21b. The interior temperature value of paste increase with aggrandizing DEC voltage, and the interior temperature of pastes DMP-8 and DMP-5 cured in 24V are 33.025°C and 42.525°C, respectively. The relationships between compressive strength, and maximum heating are presented in Fig. 21c. It indicates that the 3-d and 28-d compressive strengths has a good linear relationship with heating. The above-mentioned results further verify that the higher DEC voltage can promote the cement hydration by thermal effects.

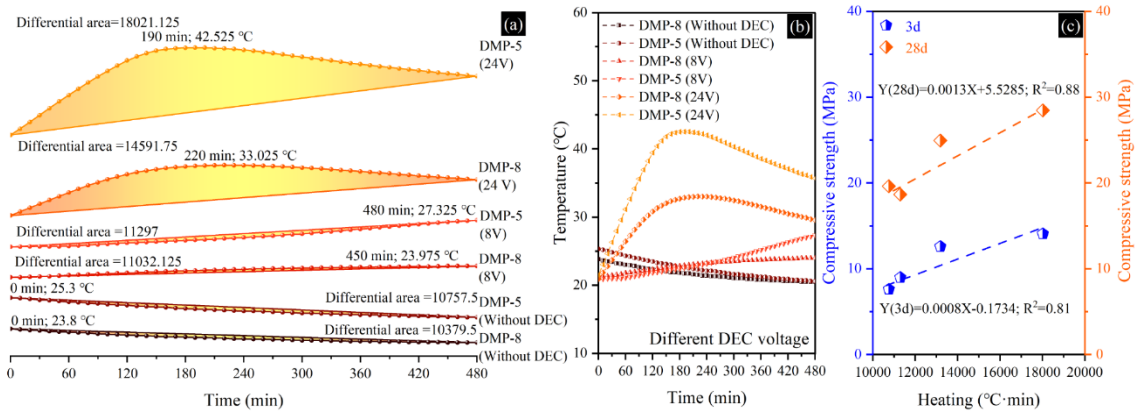

Fig. 21. Thermal effects of DEC with different voltages and IC on pastes DMP-8 and DMP-5 (a)

differential area, (b) temperature curves and (c) relationship between strength and heating

4.2 DEC power and unit resistivity

The patterns of DEC power in pastes with different cement equivalents cured in DEC with different DEC voltages are presented in Fig.22. DEC power is the other parameter for reflecting the influence of DEC on cement pastes. The calculation of DEC power according to the equation P=UI, and the electric current of selected pastes are detected by transducers. The increase in initial DEC powder of pastes as the cement equivalent increase, and the same tendency also exists in the results of differential area. The different areas for the DEC powder of pastes DMP-5 and DMP-0 are 261.54 and 682.66, respectively. The reason for this phenomenon is in accordance with that in strength and thermal effects. The DEC power increase with the increasing DEC voltage, as shown in Fig.22b. And the different area pattern indicates the paste cured in 24V significant increase in the early time. It implies that the high DEC voltage can promote the cement hydration at early time.

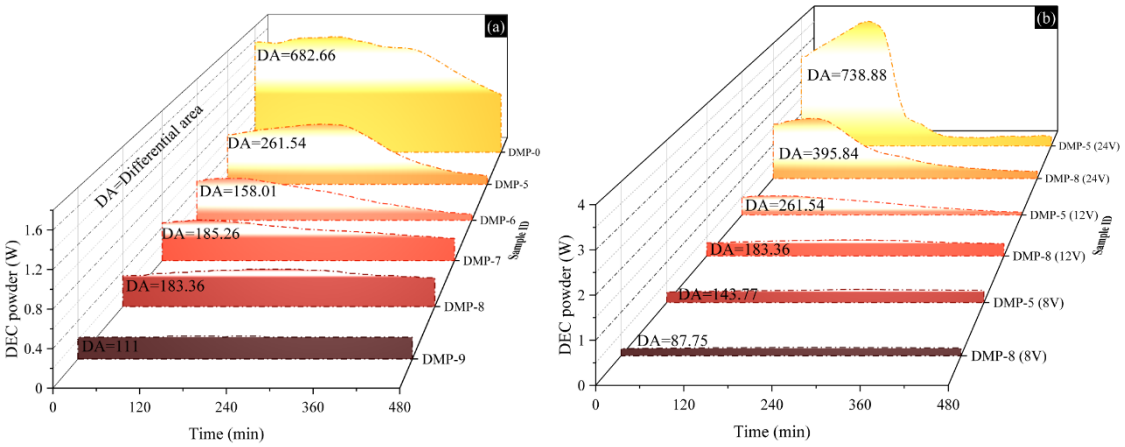

Fig. 22. Patterns of DEC power in pastes cured in DEC (a) different cement equivalents and (b) different DEC voltages

The patterns of unit resistivity in pastes DMP-8 and DMP-5 cured in DEC with different voltages are presented in Fig.23. The unit resistivity is important parameter for reflecting the effect of DEC on cement pastes. The calculation of unit resistivity according to the equation R=US/IL, where the S stands for the cross-sectional area of samples, and the L is the length of samples. The voltage and current are obtained by sensors. The increase in unit resistivity of pastes as the curing time increase, and the opposites tendency is also presented in the results of differential area of DEC power. The unit resistivity increases with the increasing DEC voltage, as shown in Fig.22b. It implies that high voltage and high cement equivalent can increase the unit resistivity as the lengthening curing time. The high

DEC with high voltage provides a thermal effect to accelerate the cement hydration, which is consistence with the above-mentioned results. In addition, with the decrease of EMR dosage, the time of significant mutation of unit resistivity is delayed. This may be related to the reaction between EMR and C_3A in cement.

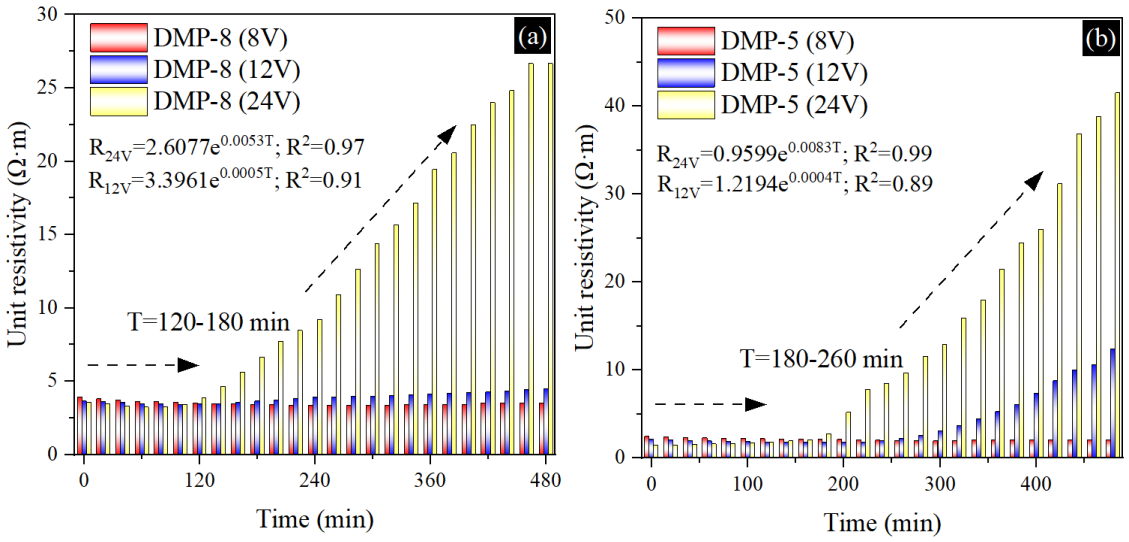

Fig. 23. Patterns of unit resistivity in pastes cured in DEC (a) DMP-8 and (b) DMP-5

4.3 Microstructure of cement-EMR pastes cured in DEC and IC

The microstructure images of cement-EMR pastes cured in DEC with different voltages and IC are shown in Fig. 24. The hydration products of all tested paste are consistence with TG-DTG results, main including ettringite, portlandite and C-S-H gels. Combination with the TG-DTG results, the portlandite, chemical binder water and hydrated degree of pastes DMP-5 cured in DEC with different voltages and IC are exhibited in Fig. 25. Portlandite is tested by the weight loss in 350~550℃, and the chemical binder water is tested by the weight loss in 0~550℃. The calculation of hydrated degree according to the equation $a=W_n/n$-LOI (Ma et al., 2021). The increase in DEC voltages can accelerate the formation of portlandite judge by the results of 8V, 12V and 24V. In other words, the weight loss obtained from portlandite in 28-d pastes cured in IC, 8V, 12V and 24V are 1.89, 2.54, 2.94 and 3.08%, respectively. In addition, the weight loss from chemical binder water of pastes cured in IC, 8V, 12V and 24V are27.33, 28.62, 28.31 and 28.97%, respectively. The large weight loss about chemical binder water can be partly explained by the high-water content of EMR. The increase in cement equivalent also facilitates the formation of portlandite and ettringite, which is attributed by more cement hydration and an increased reaction of EMR with C_3A in cement. It is noted that the application of DEC can increase the amounts of hydration products with respect to paste cured in IC, which is verified that the hydrated

degree of pastes cured in IC, 8V, 12V and 24V are 48.82, 56.39, 63.49, 70.57%, respectively.

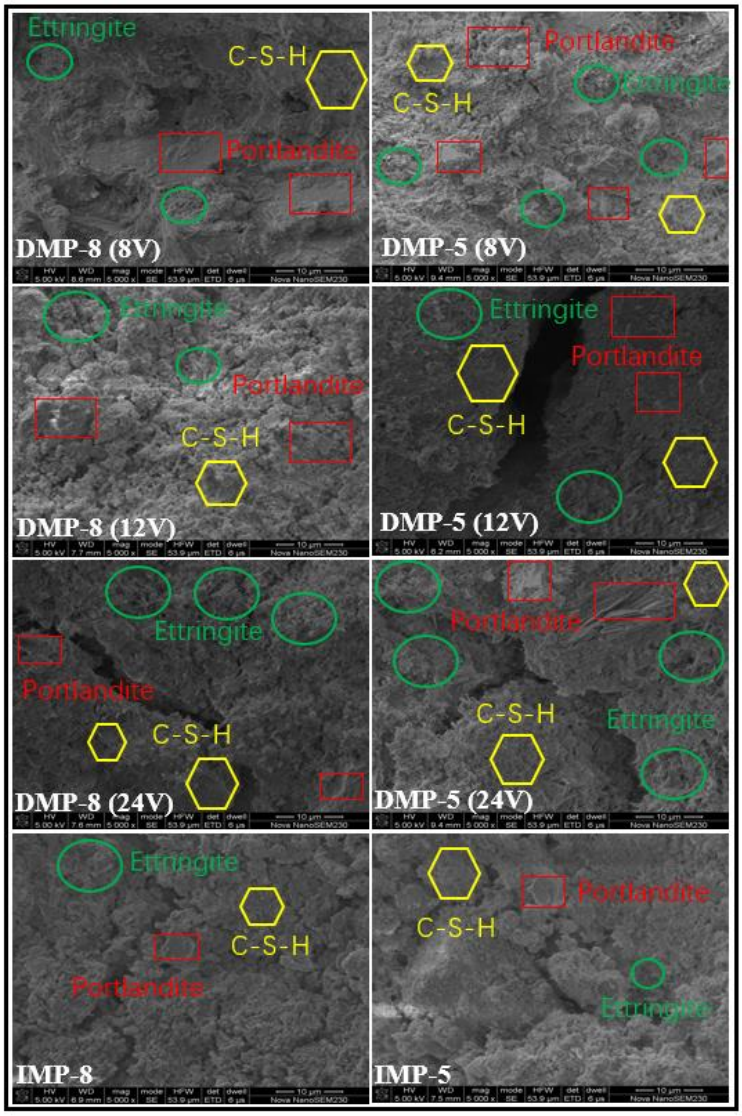

Fig. 24. Microstructure patterns of cement-EMR pastes cured in DEC with different voltages and IC

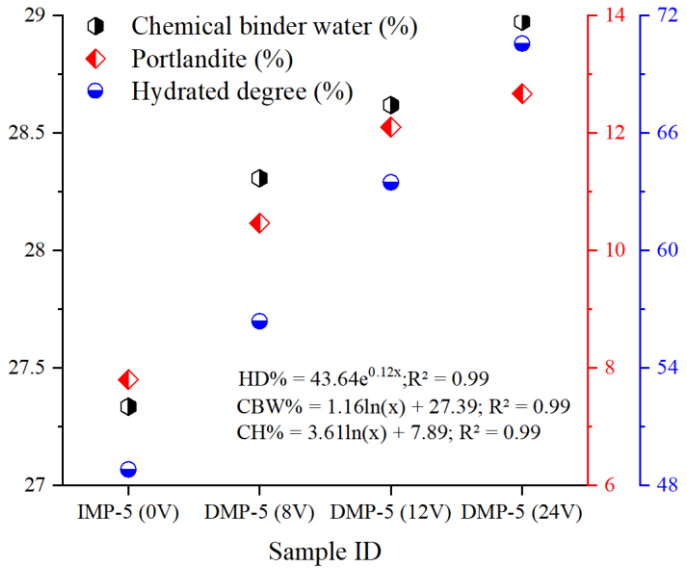

Fig. 25. Hydrated patterns of cement-EMR pastes cured in DEC with different voltages and IC

4.4 Mechanism of cement-EMR pastes cured in DEC

The application of cement for fabricating cement-EMR paste is an economical and high-efficiency method for realizing high-value resource utilization of EMR. And the application of DEC for curing cement pastes is a clean and low-carbon strengthening solution. Thus, the synergistic cement hardening and DEC is a promising method for solid waste disposal, i.e., EMR (Fig. 25). Therefore, the effects of EMR and DEC on the cement hydration deserves to be explored in-depth. From the aforementioned results, it can be seen that the hydration products of cement-EMR pastes are not significantly changed, which still mainly includes C-S-H gels, portlandite, ettringite and other incompletely reacted cement clinker. However, the main difference in cement-EMR paste is that the variation in the amount of hydration products. The effects of EMR and DEC on cement hydration can be divided into two main aspects. The first aspect is the cement hardening, in which the gypsum phase introduced by the EMR reacts with C_3A in the cement by hydration to form ettringite (Eq. (4)). In the presence of gypsum, C_3A hydrates reacts with gypsum to form high-sulfur hydrated calcium sulfate (AFt, ettringite). It is a needle-like crystals, insoluble in water, that surround the particles and form a protective layer to retard hydration (Shu et al., 2018). When gypsum is depleted, C_3A also react with ettringite to produce monosulfide hydrated calcium sulfoaluminate (AFm), as shown in Eq. (5). The formation of ettringite fills the pores in the paste and promotes the development of strength (Figs. 4, 5 and 13). Meanwhile, large amount of gypsum introduced by EMR and the low cement equivalent reduces the production of portlandite while reshapes the morphology of ettringite. The variations are not conducive to pore structure and strength.

$$3CaO\cdot Al_2O_3+3(CaSO_4\cdot 2H_2O)+26H_2O\rightarrow 3CaO\cdot Al_2O_3\cdot CaSO_4\cdot 32H_2O\cdots \quad \cdots(4)$$

$$3CaO\cdot Al_2O_3\cdot 3CaSO_4\cdot 32H_2O+2(3CaO\cdot Al_2O_3)+4H_2O\rightarrow 3(3CaO\cdot Al_2O_3\cdot CaSO_4\cdot 12H_2O)\cdots(5)$$

The second aspect is the DEC enhancing. The introduction of DEC can promote cement hydration, which is attributed from the temperature rising generated by the thermal effect. DEC takes advantage of the low resistivity of cement paste in the early-age to release a large amount of Joule heat and then promote the reaction of cement hydration (Yang et al., 2021). In addition, the increase in DEC voltage also enhances the thermal effect by improving the early-age temperature in the interior of specimens. It is noted that excessive voltage may cause thermal damage to cement paste. The maximum DEC

voltage in this paper is 24V and the tested temperature of paste is up to 42.525℃, which is not enough to cause thermal damage to the specimens.

The incorporated utilization of DEC and cement hardening is a clean and high-efficient solution for high-value and hazard-free disposal of EMR. It improves the processing capacity of EMR on the premise of ensuring good mechanical properties and removing harmful components. In other words, there are some certain limitations in the disposal of EMR with high content by cement solidification. DEC and cement curing can significantly increase the dosage of EMR for harmless disposal. In addition, from the perspective of environment and economy, this collaborative solution has some advantages to some extent. In above-mentioned results, the hydration products of cement-EMR pastes decreased due to high-dosing EMR, but the increase in DEC voltage could promote the hydration reaction of cement. In terms of toxicity leaching results, the combination of DEC and cement hardening can significantly reduce the leaching values of Mn^{2+} and NH_4^+-N. In conclusion, the incorporation of DEC and cement-solidified disposal for EMR could provide a potential solution for high-value and large-capacity disposal of hazardous solid waste.

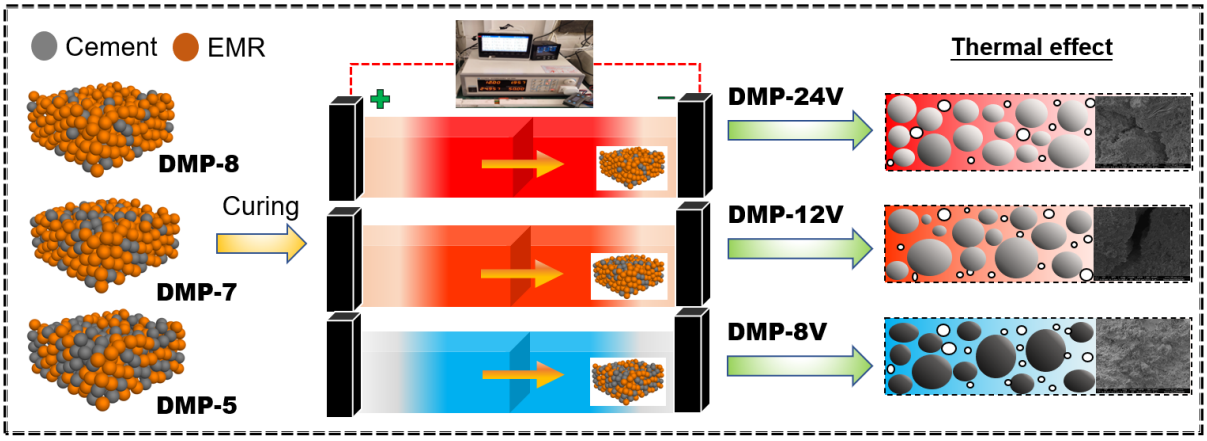

Fig.25. Schematic diagram of cement-EMR pastes cured in DEC.

5. Conclusions

(1) Cement-EMR pastes cured in DEC can increase strength with respect to that cured in IC. The increase in cement equivalent can increase strength of cement-EMR pastes cured in 12V-DEC and IC. When the cement equivalent is higher than 30%, the strength increments from 3-d to 28-d are remarkable. The increase in curing voltage does not improve the 3-d and 7-d strength of paste DMP-8, but significant enhance the 3-d and 7-d strength of paste DMP-5. The increase in cement equivalent can improve cement hardening effect, the increased voltage can enhance the ionic driving force.

(2) Cement-EMR Pastes cured in DEC can promote the decrease in total pore volume. The similar hysteresis loop means the pore structure and distribution of pastes cured in DEC does not happen significant change with respect to IC. Pore structure of the selected pastes are many slit holes formed by the lamellar particle accumulation. The increase in cement equivalent can significantly decreases the whole pore volume of pastes, meaning that higher cement equivalent produces more cement hydration products to fill paste holes. The increase in DEC voltage does not alter the morphology of hysteresis loop and the pore structure distribution of pastes but decrease the pore adsorption volume.

(3) DEC and cement equivalent have a significant influence on the capillary water absorption. The increase in cement equivalent and DEC voltage decreases the final cumulative volume of water permeation in both two stages. The final cumulative water permeation volume of pastes cured in DEC is lower than that cured in IC. The proportions of the tested pores in the pastes cured in IC are much higher than that cured in DEC based on results of water migration rate. The proportions of pores in the pastes cured in high-voltage DEC and high cement equivalent are higher than that in low-voltage and low cement equivalent.

(4) Pastes cured in DEC can promote the cement hydration than that cured in IC based on the variations in CH content. As the DEC voltage rising from 8V to 12V, the dehydration amount of C-S-H gels and ettringite (AFt) is significant increase, but the amount of CH does not change remarkable. And the same tendency presented when the voltage further rising to 24V. The same tendency does not change with changing the cement equivalent. All pastes cured in DEC does not change the types of hydration products with respect to IC. The boosted ettringite formation occurs in cement-EMR paste after introducing DEC and amplifying the DEC voltage. The improvement of ion concentration in DEC acts on accelerator to increase the hydration products.

(5) The EIF and CIF values decrease as EMR reducing from 90% to 50%, and the decrement is intimately related to the increase in strength. The EIF and CIF values of pastes DMP-5 cured in 12V-DEC exhibit the lowest values with respect to cured in other voltage and IC. When the CO_2 emission, cost and requirement of strength is considered together, DEC is the most effective and environmentally friendly method for promoting cement-EMR materials

(6) The leaching amount of Mn^{2+} and NH_4^+-N gradually decrease with the cement equivalent. The leaching amount of Mn^{2+} and NH_4^+-N of pastes cured in IC is slightly higher than that cured in DEC.

687 And the decrease in the leaching amount of Mn^{2+} and NH_4^+-N as the DEC voltage increase. This
688 tendency is consistent with results presented in pore structure and strength development. Heavy metal
689 may be embedded in the hydration products or form precipitates with other ions. In addition, the dense
690 structure of the mortar prevents the leaching behavior of heavy metal. Cement hardening is not
691 significant at early-age cement solidification, but the 28-d results showed that Mn^{2+} and NH_4^+-N in
692 were in accordance with the leaching national standards (GB 8978-1996).
693 In conclusion, the incorporation of DEC and cement-solidified disposal for EMR could provide a
694 potential solution for high-value and large-capacity disposal of hazardous solid waste.

695 ## Conflicts of interest

696 The authors declare no competing financial interests.

697 ## Acknowledgements

698 The authors appreciate the financial support from Hunan Province Key Field R&D Program
699 (Grant No.2020wk2005), and the Postgraduate Scholarship, Central South University,
700 Changsha, China.

701 ## References

702 ASTM C1585-20, Standard Test Method for Measurement of Rate of Absorption of Water by
703 Hydraulic-Cement Concretes, ASTM International, West Conshohocken, PA, 2020, www.astm.org
704 Cecini, D., Austin, S. A., Cavalaro, S. H., Palmeri, A., 2018. Accelerated electric curing of steel-fibre
705 reinforced concrete. Cons. Build. Mater., 189, 192-204. doi.org/10.1016/j.conbuildmat.2018.08.183
706 Chen, H., Long, Q., Zhang, Y., Wang, S., Deng, F., 2020. A novel method for the stabilization of soluble
707 contaminants in electrolytic manganese residue: Using low-cost phosphogypsum leachate and
708 magnesia/calcium oxide. Ecotoxicol Environ Saf. 194, 110384. doi.org/10.1016/j.ecoenv.2020.110384
709 Duan, N., Fan, W., Changbo, Z., Chunlei, Z., Hongbing, Y., 2010. Analysis of pollution materials
710 generated from electrolytic manganese industries in China. Resour Conserv Recy. 54, 506-511.
711 doi.org/10.1016/j.resconrec.2009.10.007
712 Duan, N., Dan, Z., Wang, F., Pan, C., Zhou, C., Jiang, L., 2011. Electrolytic manganese metal industry
713 experience based China's new model for cleaner production promotion. J Clean Prod. 19, 2082-2087.

doi.org/10.1016/j.jclepro.2011.06.024

Han, F., Wu, L., 2019. Resource utilization of electrolytic manganese residues, in: Industrial solid waste recycling in western China, 127-164. doi.org/10.1007/978-981-13-8086-0_3

Han, L., Wang, J., Liu, Z., Zhang, Y., Jin, Y., Li, J., Wang, D., 2020. Synthesis of fly ash-based self-supported zeolites foam geopolymer via saturated steam treatment. J Hazard Mater. 393, 122468. doi.org/10.1016/j.jhazmat.2020.122468

Han, Y., Cui, X., Lv, X., Wang, K., 2018. Preparation and characterization of geopolymers based on a phosphoric-acid-activated electrolytic manganese dioxide residue. J Clean Prod. 205, 488-498. doi.org/10.1016/j.jclepro.2018.09.141

He, D., Shu, J., Wang, R., Chen, M., Wang, R., Gao, Y., Liu, R., Liu, Z., Xu, Z., Tan, D., Gu, H., Wang, N., 2021a. A critical review on approaches for electrolytic manganese residue treatment and disposal technology: Reduction, pretreatment, and reuse. J Hazard Mater. 418, 126235. doi.org/10.1016/j.jhazmat.2021.126235

He, P., Zhu, J., Chen, Y., Chen, F., Zhu, J., Liu, M., Zhang, K., Gan, M., 2021b. Pyrite-activated persulfate for simultaneous 2,4-DCP oxidation and Cr(VI) reduction. Chem. Eng. J. 406, 126758. doi.org/10.1016/j.cej.2020.126758

He, S., Jiang, D., Hong, M., Liu, Z., 2021c. Hazard-free treatment and resource utilisation of electrolytic manganese residue: A review. J Clean Prod. 306, 127224. doi.org/10.1016/j.jclepro.2021.127224

He, S., Wilson, B. P., Lundstrom, M., Liu, Z., 2021d. Hazard-free treatment of electrolytic manganese residue and recovery of manganese using low temperature roasting-water washing process. J Hazard Mater. 402, 123561. doi.org/10.1016/j.jhazmat.2020.123561

Jiang, Y., Dai, H., Chen, Z., Liu, Y., Deng, Q., He, L., 2018. Solidification/stabilization treatment of electrolytic manganese residues and analysis of leaching toxicity. Anhui Agri. Sci. Bull. 24 (22), 131-134. doi.org/10.16377/j.cnki.issn10077731.2018.22.051 (in Chinese).

Koh, T., Hwang, S., Pyo, S., Moon, D., Yoo, H., Lee, D., 2019. Application of low-carbon ecofriendly microwave heat curing technology to concrete structures using general and multicomponent blended binder. J. Mater. Civil Eng. 31(2), 04018385.1-04018385.8. doi.org/10.1061/(asce)mt.1943-5533.0002472

743 Kovtun, M., Ziolkowski, M., Shekhovtsova, J., Kearsley, E. P., 2016. Direct electric curing of alkali-
744 activated fly ash concretes: a tool for wider utilization of fly ashes. J. Clean. Prod., 133, 220-227.
745 doi.org/10.1016/j.jclepro.2016.05.098
746 Lan, J., Dong, Y., Sun, Y., Fen, L., Zhou, M., Hou, H., Du, D., 2021. A novel method for
747 solidification/stabilization of Cd(II), Hg(II), Cu(II), and Zn(II) by activated electrolytic manganese
748 slag. J Hazard Mater. 409, 124933. doi.org/10.1016/j.jhazmat.2020.124933
749 Lan, J., Sun, Y., Tian, H., Zhan, W., Du, Y., Ye, H., Du, D., Zhang, T. C., Hou, H., 2021d. Electrolytic
750 manganese residue-based cement for manganese ore pit backfilling: Performance and mechanism. J
751 Hazard Mater. 411, 124941. doi.org/10.1016/j.jhazmat.2020.124941
752 Li, J., Du, D., Peng, Q., Wu, C., Lv, K., Ye, H., Chen, S., Zhan, W., 2018. Activation of silicon in the
753 electrolytic manganese residue by mechanical grinding-roasting. J Clean Prod. 192, 347-353.
754 doi.org/10.1016/j.jclepro.2018.04.184
755 Li, Q., Liu, Q., Peng, B., Chai, L., Liu, H., 2016. Self-cleaning performance of TiO_2-coating cement
756 materials prepared based on solidification/stabilization of electrolytic manganese residue. Cons Build
757 Mater. 106, 236-242. doi.org/10.1016/j.conbuildmat.2015.12.088
758 Li, J., Lv, Y., Jiao, X., Sun, P., Li, J., Wuri, L., Zhang, T. C., 2020. Electrolytic manganese residue
759 based autoclaved bricks with $Ca(OH)_2$ and thermal-mechanical activated K-feldspar additions. Cons
760 Build Mater. doi.org/230.10.1016/j.conbuildmat.2019.116848
761 Ma, C., Peng, J., Zhou, H., Zhou, R., Ren, W., Du, Y., 2021. An effective method for preparing high
762 early-strength cement-based materials: The effects of direct electric curing on Portland cement. J. Build.
763 Eng. 43, 102485. doi:10.1016/j.jobe.2021.102485
764 Ma, M., Du, Y., Bao, S., Li, J., Wei, H., Lv, Y., Song, X., Zhang, T., Du, D., 2020. Removal of cadmium
765 and lead from aqueous solutions by thermal activated electrolytic manganese residues. Sci Total
766 Environ. 748, 141490. doi.org/10.1016/j.scitotenv.2020.141490
767 Makul, N., Rattanadecho, P., Pichaicherd, A., 2017. Accelerated microwave curing of concrete: a
768 design and performance-related experiments. Cem. Concr. Compos., 83, 415-426.
769 doi.org/10.1016/j.cemconcomp.2017.08.007
770 Senneca, O., Cortese, L., Di Martino, R., Fabbricino, M., Ferraro, A., Race, M., Scopino, A., 2020.
771 Mechanisms affecting the delayed efficiency of cement based stabilization/solidification processes. J.

Clean. Prod. 261,121230. doi.org/ 10.1016/j.jclepro.2020.121230 121230

Shi, Y., Long, G., Ma, C., Xie, Y., He, J., 2019. Design and preparation of Ultra-High Performance Concrete with low environmental impact. J. Clean. Prod. 214, 633-643. doi.org/10.1016/j.jclepro.2018.12.318

Shu, J., Li, B., Chen, M., Sun, D., Wei, L., Wang, Y., Wang, J., 2020. An innovative method for manganese (Mn^{2+}) and ammonia nitrogen (NH_4^+-N) stabilization/solidification in electrolytic manganese residue by basic burning raw material. Chemosphere. 253, 126896. doi.org/10.1016/j.chemosphere.2020.126896

Shu, J., Liu, R., Liu, Z., Chen, H., Du, J., Tao, C., 2016. Solidification/stabilization of electrolytic manganese residue using phosphate resource and low-grade MgO/CaO. J Hazard Mater. 317, 267-274. doi.org/10.1016/j.jhazmat.2016.05.076

Shu, J., Wu, H., Chen, M., Peng, H., Li, B., Liu, R., Liu, Z., Wang, B., Huang, T., Hu, Z., 2019. Fractional removal of manganese and ammonia nitrogen from electrolytic metal manganese residue leachate using carbonate and struvite precipitation. Water Res. 153, 229-238. doi.org/10.1016/j.watres.2018.12.044

Shu, J., Wu, H., Liu, R., Liu, Z., Li, B., Chen, M., Tao, C., 2018. Simultaneous stabilization/solidification of Mn^{2+} and NH_4^+-N from electrolytic manganese residue using MgO and different phosphate resource. Ecotoxicol Environ Saf. 148, 220-227. doi.org/10.1016/j.ecoenv.2017.10.027

Standards, 1996. The State Bureau of Environmental Protection and The State Bureau of Technical Supervision. Identification standard for hazardous wastes-Identification for extraction procedure toxicity. The State Standard of the People's Republic of China, GB 5085.3-1996, Standards Press of China, Beijing. [in Chinese]

Standards, 2000. The State General Administration of the People's Republic of China for Quality Supervision and Inspection and Quarantine. Methods for chemical analysis of aluminate cement. The State Standard of the People's Republic of China, GB/T 205-2000, Standards Press of China, Beijing. [in Chinese]

Standards, 2007. The State Environmental Protection Administration. Solid waste-Extraction procedure for leaching toxicity-Acetic acid buffer solution method. The People's Republic of China

Environmental Protection Industry Standards, HJ/T 300-2007, China Environmental Science Press, Beijing. [in Chinese]

Standards, 2009a. The Ministry of Environmental Protection. Water quality-Determination of cyanide-Volumetric and spectrophotometry method. The People's Republic of China Environmental Protection Industry Standards, HJ 484-2009, China Environmental Science Press, Beijing. [in Chinese]

Standards, 2009b. The Ministry of Environmental Protection. Water quality-Determination of ammonium nitrogen-Nessler's reagent spectrophotometry. The People's Republic of China Environmental Protection Industry Standards, HJ 535-2009, China Environmental Science Press, Beijing. [in Chinese]

Standards, 2010. The Ministry of Environmental Protection. Solid waste-Extraction procedure for leaching toxicity-Horizontal vibration method. The State Standard of the People's Republic of China, HJ-557-2010, China Environmental Science Press, Beijing. [in Chinese]

Sun, D., Yang, L., Liu, N., Jiang, W., Jiang, X., Li, J., Yang, Z., Song, Z., 2020. Sulfur resource recovery based on electrolytic manganese residue calcination and manganese oxide ore desulfurization for the clean production of electrolytic manganese. Chinese J Chem Eng. 28, 864-870. doi.org/10.1016/j.cjche.2019.11.013

Tang, P., Zhang, W., Chen, Y., Chen, G., Xu, J., 2020. Stabilization/solidification and recycling of sediment from Taihu Lake in China: engineering behavior and environmental impact. Waste Manag. 116, 1-8. doi.org/10.1016/ j.wasman.2020.07.040.

Thommes, M., Kaneko, K., Neimark, A. V., Olivier, J. P., Rodriguez-Reinoso, F., Rouquerol, J., Sing, K. S., 2015. Physisorption of gases, with special reference to the evaluation of surface area and pore size distribution (IUPAC Technical Report). Pure. Appl. Chem. 87(9-10), 1051-1069. doi:10.1515/pac-2014-1117

Wadhwa, S. S., Srivastava, L. K., Gautam, D. K., Chandra, D., 1987. Direct electric curing of in situ concrete. Build. Res. Inf. 15(1-6), 97-101. doi:10.1080/09613218708726799

Wang, D., Wang, Q., Xue, J., 2020. Reuse of hazardous electrolytic manganese residue: Detailed leaching characterization and novel application as a cementitious material. Resour Conserv Recy. 154, 104645. doi.org/10.1016/j.resconrec.2019.104645

Wang, J., Peng, B., Chai, L., Zhang, Q., Liu, Q., 2013. Preparation of electrolytic manganese residue-

ground granulated blastfurnace slag cement. Powder Technol. 241, 12-18. doi.org/10.1016/j.powtec.2013.03.003

Wang, L., Yu, K., Li, J., Tsang, D.C.W., Poon, C.S., Yoo, J.C., Baek, K., Ding, S., Hou, D., Dai, J., 2018. Low-carbon and low-alkalinity stabilization/solidification of high-Pb contaminated soil. Chem. Eng. J. 351, 418-427. doi.org/10.1016/ j.cej.2018.06.118

Wang, N., Fang, Z., Peng, S., Cheng, D., Du, B., Zhou, C., 2016. Recovery of soluble manganese from electrolyte manganese residue using a combination of ammonia and CO_2. Hydrometallurgy. 164, 288-294. doi.org/10.1016/j.hydromet.2016.06.019

Wang, Y., Gao, S., Liu, X., Tang, B., Mukiza, E., Zhang, N., 2019. Preparation of non-sintered permeable bricks using electrolytic manganese residue: Environmental and NH_3-N recovery benefits. J Hazard Mater. 378, 120768. doi.org/10.1016/j.jhazmat.2019.120768

Xu, F., Jiang, L., Dan, Z., Gao, X., Duan, N., Han, G., 2014. Water balance analysis and wastewater recycling investigation in electrolytic manganese industry of China - A case study. Hydrometallurgy 149, 12-22. doi.org/10.1016/j.hydromet.2014.05.002

Xu, L. J., Wang, X. M., Chen, H. C., Liu, C. L., 2011. Mn forms and environmental impact of electrolytic manganese residue. Adv Mater Res. 183-185, 570-574. doi.org/10.4028/www.scientific.net/AMR.183-185.570

Xu, Y., Liu, X., Zhang, Y., Tang, B., Mukiza, E., 2019. Investigation on sulfate activation of electrolytic manganese residue on early activity of blast furnace slag in cement-based cementitious material. Cons. Build. Mater. 229, 116831. doi.org/10.1016/j.conbuildmat.2019.116831

Yang, Z., Xie, Y., He, J., Zeng, X., Ma, K., Long, G., 2021. Experimental investigation on mechanical strength and microstructure of cement paste by electric curing with different voltage and frequency. Con. Build. Mater. 299, 123615. doi:10.1016/j.conbuildmat.2021.12361

Zhan, X., Wang, L., Wang, L., Wang, X., Gong, J., Yang, L., Bai, J., 2019. Enhanced geopolymeric co-disposal efficiency of heavy metals from MSWI fly ash and electrolytic manganese residue using complex alkaline and calcining pretreatment. Waste Manag. 98, 135e143. doi.org/10.1016/ j.wasman.2019.08.024

Zhang, R., Ma, X., Shen, X., Zhai, Y., Zhang, T., Ji, C., Hong, J., 2020a. Life cycle assessment of electrolytic manganese metal production. J Clean Prod. 253, 119951.

doi.org/10.1016/j.jclepro.2019.119951

Zhang, W., Cheng, C., 2007. Manganese metallurgy review. Part I: leaching of ores/ secondary materials and recovery of electrolytic/chemical manganese dioxide. Hydrometallurgy 89, 137e159. doi.org/10.1016/j.hydromet.2007.08.010.

Zhang, Y., Liu, X., Xu, Y., Tang, B., Wang, Y., 2020b. Preparation of road base material by utilizing electrolytic manganese residue based on Si-Al structure: Mechanical properties and Mn^{2+} stabilization/solidification characterization. J Hazard Mater. 390, 122188. doi.org/10.1016/j.jhazmat.2020.122188

Zhang, Y., Liu, X., Xu, Y., Tang, B., Wang, Y., Mukiza, E., 2019a. Synergic effects of electrolytic manganese residue-red mud-carbide slag on the road base strength and durability properties. Constr Build Mater. 220, 364-374. doi.org/10.1016/j.conbuildmat.2019.06.009

Zhang, Y., Liu, X., Xu, Y., Tang, B., Wang, Y., Mukiza, E., 2019b. Preparation and characterization of cement treated road base material utilizing electrolytic manganese residue. J Clean Prod. 232, 980-992. doi.org/10.1016/j.jclepro.2019.05.352

Zhou, C., Du, B., Wang, N., Chen, Z., 2014. Preparation and strength property of autoclaved bricks from electrolytic manganese residue. J Clean Prod. 84, 707-714. doi.org/10.1016/j.jclepro.2014.01.052